Contract No:

This document was prepared in conjunction with work accomplished under Contract No. DE-AC09-08SR22470 with the U.S. Department of Energy (DOE) Office of Environmental Management (EM).

Disclaimer:

We put science to work.™

Savannah River National Laboratory™

OPERATED BY SAVANNAH RIVER NUCLEAR SOLUTIONS

A U.S. DEPARTMENT OF ENERGY NATIONAL LABORATORY • SAVANNAH RIVER SITE • AIKEN, SC

Vapor-Liquid Partitioning of Methylmercury Compounds: Fundamental Data to Support the Savannah River Site Liquid Waste System

Henry's Law, Solubility and Vapor Pressure Determination for Representative Methylmercury Compounds

B.B. Looney

H.H. VerMeulen

J.O. Dickson

T.L. White

A.J. Boggess

T.B. Peters

E.D. Fabricatore

June 2021

SRNL-STI-2020-00407, Revision 0

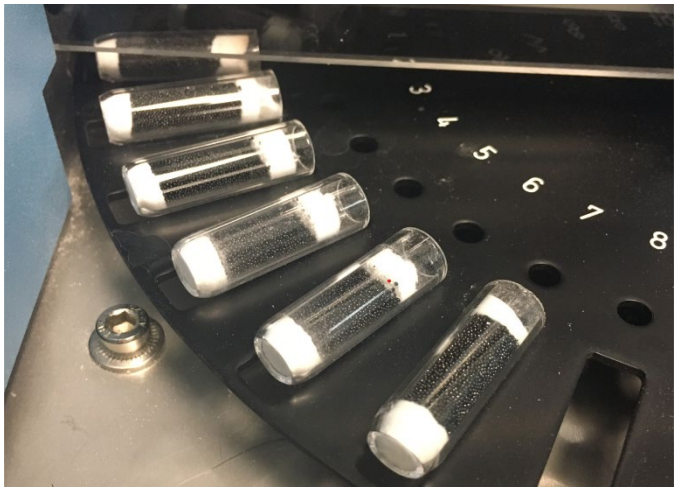

SRNL.DOE.GOV

Cover photograph: Mercury columns (Adsoquick™) used to trap mercury in gas samples; loaded onto autosampler carousel of the Milestone DMA-80™ for analysis.

Dedication: This report is dedicated to Bill Wilmarth who was the SRNL lead for mercury research for many years before he recently passed. Bill requested that we follow up on liquid-air partitioning of methylmercury after evaporative loss of methylmercury was observed in sample boats awaiting analysis in SRNL. Bill encouraged a breadth and diversity of ideas in his collaborating teams with the goal of providing creative-actionable-disciplined research. Under Bill's guidance, SRNL advanced the technical basis for managing the mercury challenges facing the SRS Liquid Waste System and generated high level of support to DOE and to the Liquid Waste Contractor - Savannah River Remediation.

Acknowledgement: This research was funded by the Department of Energy Office of Environmental Management (EM 3.2 Technology Development). The authors are grateful for the efforts of Courtney Burckhalter, Kandice Miles, Holly Hall, Austin Coleman, and Katherine Miles who provided critical support for this research. The authors gratefully acknowledge the helpful review/concurrence from the technical experts in the Savannah River Site Liquid Waste Contractor (Savannah River Remediation), including Ryan McNew, Vijay Jain, and Thomas Britt.

Printed in the United States of America

Prepared for
U.S. Department of Energy

SRNL-STI-2020-00407
Revision 0

Keywords: *headspace, Henry's Law, Liquid Waste System, mercury, methylmercury, partitioning, solubility, vapor pressure*

Retention: *Permanent*

Vapor-Liquid Partitioning of Methylmercury Compounds: Fundamental Data to Support the Savannah River Site Liquid Waste System

Henry's Law, Solubility and Vapor Pressure Determination for Representative Methylmercury Compounds

B.B. Looney
H.H. Vermeulen
J.O. Dickson
T.L. White
A.J. Boggess
T.B. Peters
E.D. Fabricatore

June 2021

Prepared for the U.S. Department of Energy under contract number DE-AC09-08SR22470.

REVIEWS AND APPROVALS

AUTHORS:

B.B. Looney, Environmental Materials and Energy Sciences Date

H.H. VerMeulen, Environmental Sciences and Dosimetry Date

J.O. Dickson, Florida International University Date

T.L. White, Spectroscopy, Separations, and Materials Characterization Date

A.J. Boggess, Spectroscopy, Separations, and Materials Characterization Date

T.B. Peters, Spectroscopy, Separations, and Materials Characterization Date

E.D. Fabricatore, Environmental Sciences and Dosimetry Date

Note: Digital and physical signatures are considered Personally Identifiable Information (PII); Approval signatures for this document are securely and permanently maintained in the SRNL Electronic Laboratory Notebook System (T6751-00178-11)

TECHNICAL REVIEW:

C.A. Eddy-Dilek, Environmental Materials and Energy Sciences Date

APPROVAL:

B. Lee, Manager Date
Environmental Materials and Energy Sciences

B.J. Wiedenman, Manager Date
Chemical Processing Technology

EXECUTIVE SUMMARY

This report explores physical and chemical behaviors of methylmercury. Methylmercury, a cation in solution, comprises a significant fraction of the mercury in the Savannah River Site (SRS) Liquid Waste System (LWS); thus, understanding physical partitioning and chemical behaviors of methylmercury is essential to support strategic, technically-based management of mercury in the LWS. As an ion, methylmercury has generally been assumed to be constrained to the liquid phase in the LWS. Therefore, it would be further assumed that this species would not be significant in the vapor phase. This conceptualization was challenged when a significant loss of methylmercury from sample boats occurred while awaiting analysis at room temperature. Follow-up studies confirmed that methylmercury is not completely constrained to the liquid phase (aqueous solution) but has a measurable partitioning into the gas phase. Based on these observations, further study on methylmercury partitioning for compounds and conditions that might be relevant to the SRS LWS were conducted, i.e., how much methylmercury might volatilize in the evaporators and then condense in the overheads. Our studies were done as a function of temperature and findings suggest that there is an increase of three to four orders of magnitude in partitioning into the vapor phase as temperatures increase from ambient (20 ˚C) to the boiling point of aqueous solutions (near/above 100 ˚C). The experiments generated data that will allow better assessment of the partitioning of methylmercury as a function of temperature: a) for methylmercury hydroxide in simulants and in solutions of varying ionic strength, b) for methylmercury sulfate, c) for methylmercury chloride in solutions of varying pH, and d) for methylmercury glycolate. The primary partitioning parameter of interest for the SRS LWS is the dimensionless Henry's Law coefficient (H') -- higher H' corresponds to more of the compound partitioning into the vapor phase. In this study, H' was measured for all compounds. For methylmercury chloride, methylmercury sulfate, and methylmercury glycolate (those compounds that precipitated in the microcosms), the associated vapor pressure and solubility were also determined.

The data were collected using a streamlined static headspace analysis strategy in replicate microcosms (sealed vials). For each vial and condition, the methylmercury partitioning between a solution and gas phase was measured. Gas and liquid subsamples were quantified using SRNL-developed, optimized methods that rely on direct mercury analysis as the final quantification step. Over 200 individual sample results were generated during the study. Key highlights of the results include:

- At 20 ˚C, the partitioning, vapor pressure, and solubility measurements in this study closely matched the available scientific literature. In dilute solutions, the H' for methylmercury hydroxide was about four orders of magnitude lower than the H' for methylmercury chloride. These compounds bracket the expected range of H' for methylmercury compounds partitioning from aqueous solution into a gas phase.
- The H' for methylmercury hydroxide increased significantly as a function of ionic strength, documenting a "salting out" effect. The H' value in the high ionic strength microcosms increased by about two orders of magnitude. In the high ionic strength trial, the measured H' closely matched the values measured in the LWS simulant solutions.
- The H' increased as a function of increasing temperature and the relationship can be reasonably described using the Van't Hoff equation. The measured vapor pressures increased as a function of temperature and the relationship can be reasonably described using the August equation. The measured solubilities increased as a function of temperature and the relationship can be reasonably described using an estimated enthalpy of solution.

- Importantly, as temperature increased, the estimates for H' trended to a similar and consistent value/magnitude for all compounds, ionic strengths, and pHs. This inherent robustness in the emergent data is significant because it provides parameter estimates for many LWS conditions that will be insensitive to specific solution conditions. At 40 ˚C, 80 ˚C, and >100 ˚C, for example, nominal estimates of H' for any LWS solution would be approximately $3x10^{-6}$, 10^{-4}, and 10^{-3}, respectively.
- A few hypothetical examples illustrate how this information might be applied in the LWS. Based on the nominal H' of $3x10^{-6}$ at 40 °C applied to a hypothetical warm-ambient waste tank with a liquid phase methylmercury concentration of 100 mg/L (100,000 µg/L) as Hg, the calculated equilibrium methylmercury concentration in the headspace gas would be relatively low -- about 0.3 µg/L. For context, this hypothetical value is lower than the measured headspace gas levels of elemental mercury (about 10 µg/L as Hg in some LWS tanks). Under hypothetical evaporator conditions with temperatures exceeding 100 °C, a nominal H' of 10^{-3} and similar liquid concentrations, the equilibrium gas phase concentration of methylmercury over the heated liquid would be higher -- in the range of 100 µg/L. The physical partitioning of methylmercury in an evaporator system results from many complex and interacting factors (distillation and partitioning processes, liquid and gas volumes and flows, etc.) and the overall behavior of methylmercury in the system can also be influenced by chemical processes and potential for methylmercury formation or degradation. The availability of more definitive partitioning information may facilitate and improve future evaluations of methylmercury behavior in the heated evaporators.

This research was primarily intended to provide parameters for Savannah River Remediation (SRR) and LWS scientists and engineers to make flowsheet and design calculations. However, an additional potentially significant finding was identified while performing the experiments. In microcosms where methylmercury was added in the presence of formate, significant quantities of dimethylmercury were synthesized in the aqueous solution and partitioned into the headspace. The fugacity of mercury species in the formate microcosms was significantly higher than expected; orders of magnitude higher than that of methylmercury glycolate, methylmercury chloride, and methylmercury hydroxide. The unexpected finding was validated by independent analysis and a conjectural reaction mechanism for the formation of dimethylmercury was developed. The observed synthesis of dimethylmercury by reaction of methylmercury and formate is described in detail to help inform future flowsheet engineering and management (e.g., gylcolate versus formate) and provide insight into this mechanism as a potential contributor to the observations that trace levels of dimethylmercury are being measured by SRR industrial hygienists in the headspace of some of the key waste tanks.

TABLE OF CONTENTS

LIST OF TABLES

LIST OF FIGURES

LIST OF ABBREVIATIONS

$(CH_3)_2Hg$	Dimethylmercury
CH_3Hg^+	Methyl mercury
CH_3HgCl	Methyl mercuric chloride or (mono)methylmercury chloride salt
CH_3HgOH	(Mono)methylmercury (II) hydroxide or methyl mercuric hydroxide
CH_3HgNO_3	Methyl mercuric nitrate
$(CH_3Hg)_2S$	Dimethylmercury sulfide
DI	Deionized
DMA	Direct mercury analyzer (Milestone DMA-80)
DWPF	Defense Waste Processing Facility
EPA	Environmental Protection Agency
EPI	Estimation Program Interface
GC-MS	Gas chromatography- mass spectroscopy
Hg	Mercury
Hg^0	Elemental mercury
Hg^{2+}	Divalent mercury
$HgCl_2$	Mercuric chloride
HgS	Metacinnabar
H, H', H_{cc}, H_{pc}, H_{xx}, H_{px}	Henry's Law coefficient (superscripts and subscripts denote various units as described in the report)
LFL	Lower Flammability Limit
LWS	Liquid waste system
$NaBH_4$	Sodium borohydride
NMR	Nuclear magnetic resonance
PVDF	Polyvinylidene fluoride
$SnCl_2 \cdot 2H_2O$	Stannous chloride dihydrate
SRNL	Savannah River National Laboratory
SRR	Savannah River Remediation
SRS	Savannah River Site

1.0 Introduction and Basis for Work

The Savannah River Site (SRS) Liquid Waste System (LWS) contains approximately 66 tons of mercury within the liquids, salts, and sludges that are currently being processed into final wasteforms for disposal. Mercury concentrations within the system exceed those typically experienced in environmental or industrial systems; thus, management of mercury compounds continues to be a priority for SRS. In the LWS, waste is vitrified into a borosilicate glass wasteform that contains most of the radioactivity, while the lower activity solutions are dispositioned in a low-level grout wasteform, or "saltstone". The alkaline, high ionic strength caustic wastes are pumped, evaporated, and otherwise managed throughout the LWS and Defense Waste Processing Facility (DWPF) as they are stored and prepared for conversion to the final wasteforms. Because of the complexity of this system, a key component of effective mercury management in the LWS requires analysis of mercury in various physical phases. The high concentration of mercury within the SRS LWS has the potential to generate vapor-phase contamination. Elemental mercury (Hg^0), dimethylmercury ($(CH_3)_2Hg$), and methylmercury (CH_3Hg^+) are among species known or suspected to contribute to the flux of mercury from liquid to vapor phase (Iverfeldt and Lindquist, 1982). Chemical speciation affects not only mercury behavior in LWS operations but may also affect the performance of mercury treatment and removal technologies in the LWS.

Previous analyses identified the formation of $(CH_3)_2Hg$ in the LWS and suggested it is being produced from organic materials containing methyl groups, such as antifoam agents, within the waste tanks (Bloom et al., 2004). Continuous generation of $(CH_3)_2Hg$ in situ is supported by detectable concentrations found during evaporation, coupled with the expected short half-life (Bloom et al., 2004). In addition to $(CH_3)_2Hg$, CH_3Hg^+ has also been detected as a significant dissolved species in LWS fluids (Meraw, 2015).

CH_3Hg^+ can be formed by both biotic and abiotic processes. In environmental conditions such as wetlands, lakes, and streams, anaerobic bacteria species are able to convert mercury species into CH_3Hg^+, while other bacteria and plants can breakdown the compound. CH_3Hg^+ degradation by biotic factors often results in the formation of Hg^0 and additional products such as methane or carbon dioxide (Kanzler et al., 2017). Mercury speciation is also influenced by the presence of sulfides and other functional groups in anaerobic environments.

Previous studies in the SRS LWS document that abiotic methylation of Hg(II) in the unique high pH waste solutions can produce significant quantities of CH_3Hg^+. Subsequent addition of a second methyl group may then result in formation of $(CH_3)_2Hg$, but this would occur less rapidly than the initial methylation and translate to the lower overall concentrations of that species in the LWS (Bloom, 2004).

This report explores the basic physical and chemical behaviors of CH_3Hg^+ in an effort to support technically based management of this important mercury species during waste disposal activities. Recent observations indicate that CH_3Hg^+ is not constrained to the liquid phase in the LWS. This species was found to have a measurable partitioning into the gas phase at ambient conditions. Partitioning for compounds and conditions relevant to the SRS LWS were explored to determine how readily and in what quantities of CH_3Hg^+ might volatilize in the evaporators and then condense in system overheads.

Henry's Law can be used to describe the degree to which CH_3Hg^+ can be released from the liquid tank waste to the evaporators and is useful as a guide to support effective and efficient technologies for mercury treatments. Henry's Law constant (H) is a function of vapor pressure and solubility, but may be influenced by factors like pH, ionic strength, and temperature. Henry's Law is summarized in Equation 1-1 and describes the relationship between the solubility of a dissolved gas and the concentration (or partial pressure) of that gas above the liquid. Because these two factors are assumed to be proportional, a decrease in gas phase concentration above an equilibrated liquid would result in a release of the gas into the vapor

space to re-establish the Henry's Law ratio. A disequilibrium between the liquid tank waste and the air above it (e.g., in tanks or in evaporators) and a tendency for the system to then equilibrate according to Henry's Law is assumed.

$C_{gas} = H\ C_{liquid}$ ..... **Equation 1-1**

where

C_{gas} is the concentration or partial pressure of gas above the liquid
H is the Henry's Law constant of the gas
C_{liquid} is the solution concentration or mole fraction of the dissolved gas

Henry's Law is an empirical-conditional relationship that varies as a function of temperature and reactions/interactions in the solution. The units of Henry's Law vary depending on the units used for C_{gas} (the concentration in the gas phase) and C_{liquid} (the concentration in the liquid phase). According to the EPA (2021), "Henry's law coefficients can be expressed in at least four sets of units…" Units used for Henry's Law include:

H_{cc} = H' = Concentration in the gas phase / Concentration in the aqueous phase (dimensionless)
H_{pc} = Partial Pressure / Concentration (atm m3/mol)
H_{yx} = Mole Fraction Y / Mole Fraction X
H_{px} = Partial Pressure / Mole Fraction X (atmospheres)

We have highlighted in bold the most common units for Henry's Law applied to environmental engineering and environmental science applications (H' and H_{pc}). For consistency, we will use the dimensionless form of Henry's Law, H', throughout this report. Notably, if the subject solid phase is present in solution in a closed system, then the liquid will represent the conditional solubility of that solid and the gas phase concentration will represent the conditional vapor pressure; i.e.: H' ≅ vapor pressure/solubility.

The basic gas liquid partitioning relationships of potential interest for organomercury species have not been measured for typical LWS conditions, and thus values are not readily available in the literature that can be used to accurately describe this system. The gas liquid partitioning will vary depending on the media being studied and in response to a number of factors like pH, temperature, and the associated counter ions (Table 1-1).

A previous study conducted by SRR investigated the chemical characteristics of organomercury species with respect to volatility and flammability (Meraw, 2015). The study focused specifically on organomercury compounds such as dimethylmercury [$(CH_3)_2Hg$] and various methylmercury compounds [CH_3Hg^+X] that are present within the SRS Saltstone Facility and SRS LWS. Physical and chemical factors that are related to flammability (vapor pressure, H', and flammability metrics) were tabulated for several species; including, methyl mercuric chloride (CH_3HgCl), methyl mercuric hydroxide (CH_3HgOH), elemental mercury, and $(CH_3)_2Hg$ (Table 1-1). Meraw (2015) provided a significant and useful compilation of the available physical and chemical literature on organomercury and, importantly, developed a reasonable and technically based assessment of the potential for organomercury to contribute to flammability safety basis considerations. Some key conclusions from Meraw (2015) include:

- The dominant organomercury compound found in the LWS is the methyl mercury (II) cation and is likely in the form of a hydroxide or nitrate. These compounds are not sufficiently volatile to contribute to flammability risks and they should not be assumed to have the same flammability risk as $(CH_3)_2Hg$.

- $(CH_3)_2Hg$ has been detected in LWS samples, but at trace concentrations that are significantly lower than the methylmercury cation. Dimethylmercury, $(CH_3)_2Hg$, is a relatively volatile species and is the only identified mercury compound of flammability concern. Measured LWS concentrations of $(CH_3)_2Hg$ in solution are well below levels of concern, and the maximum calculated vapor phase concentrations based on Henry's Law partitioning from LWS liquids is significantly below the Lower Flammability Limit (LFL, i.e., $<< \sim 2.5$ % by volume in air).

While the literature tabulated by Meraw (2015) provided a sound basis for bounding potential flammability and safety basis risks and for determining that cationic methylmercury does not represent a flammability concern, the data does not provide sufficient information to support a more detailed understanding of the behavior of CH_3Hg^+ over the range of LWS and DWPF conditions. The data available to Meraw (2015) was generally collected at ambient temperature (20 to 25 °C) and for solution conditions that are not representative of the high ionic strength and extreme pHs in the LWS. Further, much of the literature focuses on CH_3HgCl, a compound that is not expected to be dominant in the LWS because the addition of chloride to the process is avoided by procedure and policy to minimize potential for corrosion of tanks and piping. Thus, the flammability evaluation required several bounding assumptions; like multiplying the H' for CH_3HgOH by 1000 to provide an estimate of the H' at elevated temperature in an evaporator, for example. The 2015 evaluation did not explicitly consider salting out at high ionic strength and did not consider the many ions comprising LWS solutions and simulants.

After volatilization of various methylmercury compounds from sample boats staged in the carousel of the Milestone DMA-80 awaiting analysis was observed at SRNL, Dr. Bill Wilmarth advocated and supported a focused study to measure and document an expanded set of relevant physical and chemical parameters as a resource for LWS and DWPF scientists and engineers. The specific goals of the work are to collect information on H', vapor pressure, and solubility over a range of temperatures, ionic strengths and pHs, as well as to include representative organic acids (e.g., glycolate) to determine if these would increase CH_3Hg^+ volatility. Further, the effort also includes measurements for compounds/conditions documented in the literature (e.g., CH_3HgCl and CH_3HgOH and ambient temperature) to verify and validate the protocols. Thus, this study builds on Meraw's effort through investigating additional anions and documenting the effects that temperature, ionic strength, and other solution conditions have on liquid-gas partitioning for methylmercury species.

Mercury compounds expected in SRS waste can be classified based on volatility and reactivity (Meraw, 2015). $(CH_3)_2Hg$ can be designated as volatile with a relatively high H', while both organomercuric compounds and CH_3Hg^+ are classified as nonreactive. CH_3Hg^+ is classified as not volatile due to its low vapor pressure, H value, and water solubility. This low vapor pressure causes CH_3Hg^+ to behave as a salt that is found in the vapor space in limited quantities. Similarly, the vapor pressure of compounds and complexes like CH_3HgOH and CH_3HgCl are expected to be low. Based on known properties, Meraw (2015) concluded that $(CH_3)_2Hg$ is the species most likely to be released into the vapor space at the air/water interface based on its volatility.

This work focused on augmenting the current body of literature by investigating the fundamental properties of organomercury species, including vapor pressure and solubility, and develop a more complete set of values to describe these species within SRS liquid tank wastes and associated evaporators.

Table 1-1. Literature-Reported Henry's Law Coefficients for Aqueous CH_3Hg^+ Species.

Reference	Targeted species/ application	Parameters reported	Notes
Iverfeldt and Lindqvist (1982)	Distribution of CH_3HgCl between gas phase and aqueous solution	$H'_{CH3HgCl,\ 0.7\ M\ NaHCl,\ 25\ °C} = 1.9(\pm 0.2) \times 10^{-5}$ $H'_{CH3HgCl,\ 0.1\ M\ NaHCl,\ 15\ °C} = 1.6(\pm 0.2) \times 10^{-5}$ $H'_{CH3HgCl,\ 2E(-4)\ M\ NaHCl,\ 10\ °C} = 0.94 \times 10^{-5}$	Reported H' for CH_3HgCl in various media at different temperatures
Talmi and Mesmer (1975)	Distribution of $(CH_3)_2Hg$ between air and water and the vapor pressures above CH_3HgX compounds and their solutions	$VP_{CH3HgCl,\ 22\ °C} = 0.011$ mm Hg $VP_{CH3HgCl,\ 0\ °C} = 0.00080$ mm Hg $VP_{CH3HgOH,\ 22\ °C} = 0.0056$ mm Hg $H'_{(CH3)2Hg,\ 25\ °C} = 0.31$ $H'_{CH3HgCl,\ 25\ °C} = -2.8 \times 10^{-5}$	Reported vapor pressures and H' for CH_3HgCl and CH_3HgOH
Iverfeldt and Persson (1985)	Solvation thermodynamics of methylmercury (II) species	$H'_{CH3HgOH,\ milli\text{-}Q\ water,\ pH\ 10.1,\ 15\ °C} = 1.73 \times 10^{-7}$ $H'_{CH3HgOH,\ milli\text{-}Q\ water,\ pH\ 10.1,\ 20\ °C} = 2.69 \times 10^{-7}$ $H'_{CH3HgOH,\ 2x10^{-4}\ M\ NaCl,\ pH\ 11.5,\ 11.5\ °C} = 5.27 \times 10^{-8}$ $H'_{CH3HgOH,\ 2x10^{-4}\ M\ NaCl,\ pH\ 11.5,\ 25\ °C} = 2.48 \times 10^{-7}$ $H'_{CH3HgOH,\ 0.7\ M\ NaClO4,\ pH\ 11.2,\ 20\ °C} = 3.19 \times 10^{-7}$ $H'_{CH3HgOH,\ 0.7\ M\ NaClO4,\ pH\ 11.2,\ 25\ °C} = 3.83 \times 10^{-7}$	Reported H' for CH_3HgOH starting material in various media at different temperatures
Meuleman et al. (1993)	Distribution of these species in aqueous solutions and their gas/liquid partitioning as a function of pH and halide concentration	$H'_{MeHgCl,\ 25\ °C} = 3.8 \times 10^{-5}$ $H'_{MeHgCl,\ 80\ °C} = 3.1 \times 10^{-4}$ $H'_{MeHgBr,\ 25\ °C} = 9.8 \times 10^{-5}$ $H'_{MeHgBr,\ 80\ °C} = 9.4 \times 10^{-4}$ $H'_{MeHgI,\ 25\ °C} = 5.9 \times 10^{-4}$ $H'_{MeHgI,\ 80\ °C} = 4.3 \times 10^{-3}$ $H'_{MeHgOH,\ 25\ °C} = 4 \times 10^{-6}$ $H'_{MeHgOH,\ 80\ °C} = 2.8 \times 10^{-5}$	Reported H' for CH_3HgX at different temperatures
Meraw (2015)	Chemical characteristics of organomercury compounds in SRS waste with respect to volatility and flammability	$H'_{CH3HgCl} = 5 \times 10^{-5}$ $H'_{CH3HgOH} = 5.48 \times 10^{-9}$ $H'_{(CH3)2Hg} = 0.3$ $VP_{CH3HgCl,\ 25°C} = 0.0085$ mm Hg $VP_{CH3HgOH,\ 25°C} = 0.21$ mm Hg $VP_{(CH3)2Hg,\ 25°C} = 62.37$ mm Hg (8.2 volume%)	H' and vapor pressure data tabulated from the literature
Long and Cattanach (1961)	Measurements of dimethylmercury and dimethylcadmium vapor pressure	$VP_{(CH3)2Hg,\ -11.2°C} = 8.7$ mm Hg $VP_{(CH3)2Hg,\ 0.8°C} = 17.7$ mm Hg $VP_{(CH3)2Hg,\ 8.0°C} = 26.4$ mm Hg $VP_{(CH3)2Hg,\ 23.7°C} = 58.8$ mm Hg (7.7% by volume) $VP_{(CH3)2Hg,\ 35.8°C} = 102.0$ mm Hg $VP_{(CH3)2Hg,\ 51.7°C} = 192.9$ mm Hg $VP_{(CH3)2Hg,\ 64.0°C} = 305.5$ mm Hg $VP_{(CH3)2Hg,\ 85.1°C} = 608.3$ mm Hg	Vapor pressures observed during experimentation

The US Environmental Protection Agency (EPA) assembled a toolkit that tabulates available physical and chemical data and extends the dataset where possible with thermodynamic and empirical estimation. This toolkit, the EPA Estimation Program Interface (EPI) Suite, is a Windows®-based suite of physical/chemical property and environmental fate estimation programs developed by EPA's and Syracuse Research Corporation that is free and available to the public (EPA, 2017). The objective of the EPI Suite is to provide technically based and referenceable parameters for use in environmental and process models. As a background resource for the LWS research, the relevant tabulations and estimations for included methylmercury salts/compounds is provided in Table 1-2.

Table 1-2. Summary of Parameters from EPA Estimation Programs Interface for Sample Compounds.

Compound	Chemical formula	MW	CAS No.	Log Kow (---)	Solubility at 25 °C (mg/L)	Vapor pressure at 25 °C (mm Hg)	Vapor pressure at 25 °C (Pa)	Henry's Law coefficient at 25 °C (---)	Boiling point (°C)	Hydroxyl radical rate constant (cu cm/ (molecule-sec))	notes
Methylmercury chloride	CH_3HgCl	251.1	000115-09-3	0.39 to 0.41	10,420 to 19,727	0.0085	1.34	9.33×10^{-6}	117	8.16×10^{-12}	See Henry's Law, solubility, and vapor pressure sections of report for additional information on these parameters
Methylmercury hydroxide	CH_3HgOH	232.6	001184-57-2	-1.33	1,000,000	n/a [a]	n/a	5.47×10^{-9}	182	8.30×10^{-12}	
Methylmercury cyanide	CH_3HgCN	241.6	002597-97-9	-0.85	73,359 to 200,000	n/a	n/a	5.49×10^{-9}	193	8.16×10^{-12}	
Methylmercury thiol	CH_3HgSH	248.7	054277-95-1	0.08	15,521 to 20,710	n/a	n/a	n/a	161	8.16×10^{-12}	
Methylmercury iodide	CH_3HgI	251.1	000115-09-3	0.89	1,192 to 4,363	n/a	n/a	n/a	117	8.16×10^{-12}	
Methylmercury oxyquinolate	$CH_3HgC_9H_6NO$	360	000085-85-1	1.52	270 to 1,686	n/a	n/a	1.01×10^{-10}	349	1.36×10^{-10}	

[a] n/a = not tabulated. EPI estimate for vapor pressure is unrealistic (high) and the estimate for H' was based on vapor pressure. Only measured vapor pressures and/or H' values were included in the table.

2.0 Objectives

The overarching objective of this work is to elucidate several physical-chemical properties of methylmercury cation species as a function of temperature and waste solution composition that is relevant to the complex chemistry of the SRS LWS. This is a fundamental chemistry study of Henry's Law, vapor pressure, and solubility as they relate to mercury species found in SRS tank waste solutions.

3.0 Experimental Procedure

3.1 Approach

SRNL developed and deployed an innovative strategy to generate high strength solutions of various methylmercury salts in solution for use in static headspace experiments. The strategy was necessitated by the lack of availability of high purity methyl mercury salts (solids) to use as starting materials. To overcome this limitation, a concentrated 1 M solution of CH_3HgOH in deionized (DI) water (Alfa Aesar, Item 13395) was used as the basic starting material for all testing. The CH_3HgOH stock solution is a high-quality commercial product that has been carefully vetted for purity by SRNL in previous studies. The availability of concentrated (1 M or 200,000 mg/L as Hg) stock starting solution is possible due to the high solubility of CH_3HgOH compared to other methylmercury salts. Prior to use, the methylmercury stock solution was purged with pure nitrogen (gas water ratio of 50:1) to remove any potential artifacts associated with the trace presence of volatile mercury species. This pretreatment provides for robust removal of both elemental mercury (Hg^0) and dimethylmercury ($(CH_3)_2Hg$).

For each set of microcosms, equal parts of the stock solution and a diluent/simulant were blended to generate the desired equivalent methylmercury salt or the desired simulant solution conditions. For example, blending 1 M HCl with the 1 M methylmercury hydroxide solution would result in a final solution containing 0.5 M CH_3HgCl. Note that in this scenario, the original counter-ions (H^+ and OH^-) would combine to form water, so the microcosm conditions are representative of a simple dilution of pure CH_3HgCl. A similar strategy was employed with glycolic acid, formic acid, and sulfuric acid to generate the microcosms that represent methymercury glycolate, methylmercury formate, and methylmercury sulfate, respectively. In cases where the solubility of the resulting methylmercury salt was less than 0.5 M, solids precipitated in the microcosm and the dataset could be used to generate solubility and vapor pressure, in addition to Henry's Law.

In the case of LWS simulants, the final prepared microcosms contained approximately 0.5 M methylmercury ion and a bulk solution that is generally representative of LWS conditions. The potential impacts of ionic strength were studied by extending the baseline CH_3HgOH (DI water) microcosm through the addition of excess sodium hydroxide to the vial. The final OH^- concentration in the "DI water" microcosm was approximately 0.02M; two additional ionic strength were tested with final OH^- concentrations of 0.51M ("medium" ionic strength) and 1.51m ("high" ionic strength). The pH of each microcosm was measured by placing a partial drop of solution onto pH indicator paper – the test paper was disposed as mercury waste. For species other than CH_3HgOH, the pH of the blended solutions ranged from about 5 to 11 depending on the specific acid being added, the exact normality of the different reagent grade acids, and solution interactions. After the initial blending, the pH was adjusted by adding small amounts of a 0.1M solution of the acid being tested or NaOH. For example, the pH of the CH_3HgCl microcosm was adjusted using a small quantity of additional HCl.

Following preparation of the sealed microcosms, methylmercury partitioning was evaluated using a static headspace method over a range of temperatures; typically, 22, 40 and 60 (or 70) °C. For the static headspace protocol, mercury was quantified by direct analysis of total mercury concentration (all chemical forms) in the gas and liquid phases. An implicit assumption in this protocol is that the spiked methylmercury ion is not transformed into another form of mercury (such as elemental mercury, inorganic ionic mercury or dimethylmercury). Except as noted in the results, the data generated in this study closely match the available literature measurements for methylmercury compounds, generally validating the protocol assumption and supporting the streamlined strategy.

The protocols and experiments were implemented using several sequential steps, including: a) preparation of stock solution, simulants and diluents, b) dispensing the solutions into microcosm vials (20 mL amber glass with septum lids), c) placing vials in a constant temperature water bath at 22 °C for equilibration (approximately 48 hours), d) subsampling the gas phase and the liquid phase in each microcosm using a gas tight syringe and then returning each vial to water bath, e) trapping the gas sub-sample on a mercury sorbent for analysis on the Milestone DMA-80, f) performing an initial liquid filtration using a 13 mm diameter, 0.45 µm hydrophilic PTFE membrane syringe filter and serial dilution of the liquid sample (typically 34,300 x DF) for analysis on the Milestone DMA-80, g) repeating steps c trough f for 40 °C and 60 °C, and h) working up the resulting data. Three to five replicates were performed for each microcosm condition. A total of eighteen vials could be placed in the water bath at any time so that each campaign allowed testing of four to six microcosm conditions, depending on the number of replicates used. The strategy for the experiments is straightforward and is graphically summarized in Figure 3-1. These protocols proved to be practical and reproducible. In the microcosms where solids formed, the data workup was extended to generate estimates of solubility and vapor pressure as depicted in Figure 3-2.

3.1.1 Preparation of the LWS simulant solutions

The simulated tank waste solution is predominantly a 5.6 molar sodium solution comprising of a mixture of sodium hydroxide, chloride, carbonate, nitrite, nitrate, chromate, molybdate, phosphate, sulfate, silicate, and aluminum, potassium, and cesium nitrate. The protocols were developed to test simulants with relatively higher nitrated concentrations, designated as “high nitrate simulant”, and relatively higher hydroxide concentration, designated as Table 3-1.

Table 3-1. Chemical Composition of Simulated Tank Waste Solution.

Component	High NO_3^- concentration (M)	High OH^- Concentration (M)	Average concentration (M)
Na^+	5.60	5.60	5.60
K^+	0.0041	0.030	0.015
Cs^+	0.00014	0.00037	0.00014
OH^-	1.17	3.05	1.91
NO_3^-	2.84	1.10	2.14
NO_2^-	0.37	0.74	0.52
AlO_2^-	0.32	0.27	0.31
CO_3^{2-}	0.16	0.17	0.16
SO_4^{2-}	0.22	0.030	0.15
Cl^-	0.040	0.010	0.025
F^-	0.050	0.010	0.032
PO_4^{3-}	0.010	0.008	0.010
$C_2O_4^{2-}$	0.008	0.008	0.008
SiO_3^{2-}	0.004	0.004	0.004
MoO_4^{2-}	0.0002	0.0002	0.0002

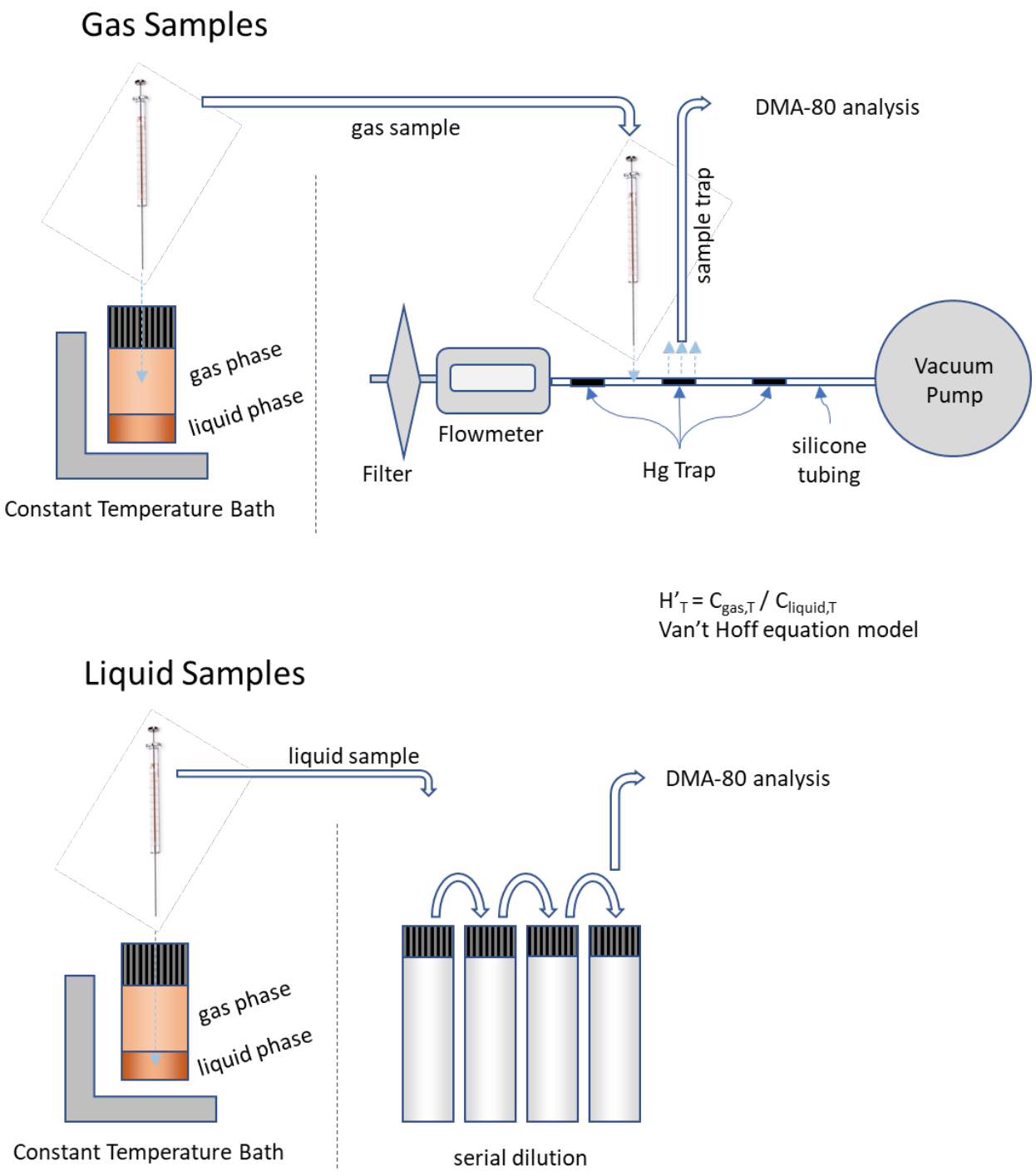

Figure 3-1. Generalized Protocols for Determining Henry's Law using Headspace Microcosms

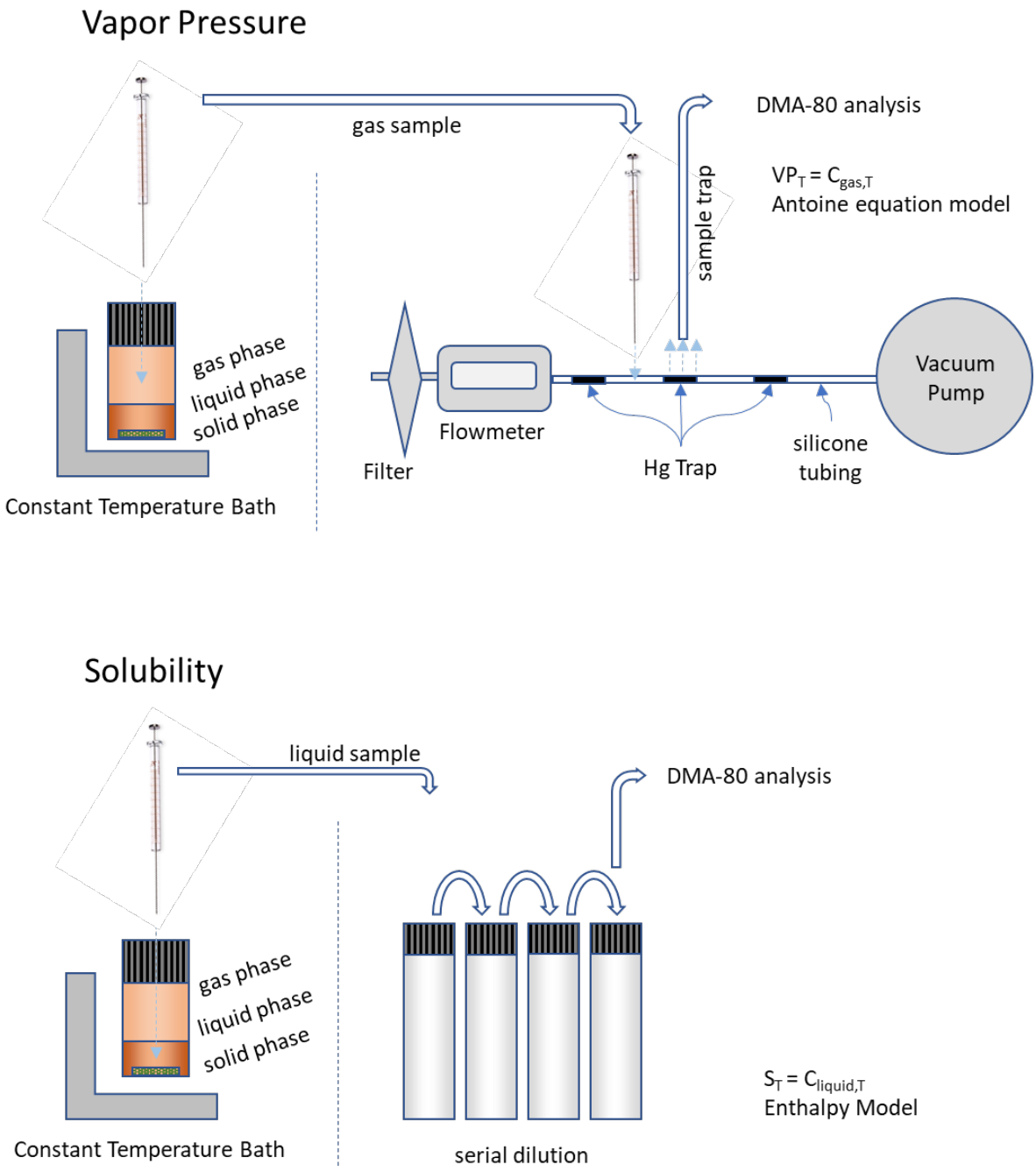

Figure 3-2. Generalized Protocols for Determining Vapor Pressure and Solubility in Microcosms Containing Precipitated Solid Methylmercury Salts

3.1.2 Mercury Analysis and Quantification

Sample analysis methods utilized in this work were adapted from EPA Method 7473, *Mercury in Solids and Solutions by Thermal Decomposition, Amalgamation, and Atomic Absorption Spectroscopy* (EPA, 2007) and performed via a Milestone Direct Mercury Analyzer (DMA-80). The DMA-80 automates the following sequential steps: pyrolysis, catalysis, amalgamation, thermal desorption, and atomic absorption spectroscopy to quantify mercury concentration in a sample. The SRNL DMA- 80 system consists of the instrument (DMA80 tri-cell) and accessory air compressor (DMA80- AC) for continuous supply of high purity mercury-free, low moisture air. Operation was performed in accordance with the manufacturer's (Milestone) manuals, SRNL R&D Directions (SRNL-RP-2018-01129), and the SRNL Hazard Analysis System (SRNL-ACT-01267). A generalized diagram of the DMA-80 used in this study is depicted Figure 3-3.

For the static headspace method, subsamples of headspace gas and liquid were collected using a Hamilton gas tight syringe. For the gas subsamples, the volume of the sample was selected to yield an approximately 5 to 100 ng of total mercury as Hg. The nominal gas volumes used for the subsampling were 200 µL, 80 µL, and 8 µL at 22, 40 and 60 °C, respectively. The gas subsamples were collected by preloading the syringe with clean flush air (approximately 10% of syringe volume), piercing the septum and collecting the desired volume, and then removing the needle and pulling in clean air (approximately 10% of the syringe volume) to limit any sample loss. For example, for a the largest sample, 25 µL of clean air was preloaded into a 250 µL syringe, the septum was pierced and a 200 µL gas sample was pulled (up to 225 µL mark), the needle was removed from the vial and the plunger was withdrawn to 250 µL to buffer the sample with clean air. The subsamples were injected into a column loading apparatus, the syringe was pumped three to 5 times to assure complete transfer. Flowing clean air within the column loading apparatus passed through a mercury sorbent trap (Milestone Adsoquick) for collection. The trap was placed into the autosampler carousel of the Milestone DMA-80. The concentration in the gas phase was calculated by dividing the mass of mercury (ng) in each subsample by the volume of gas collected (mL). The gas phase results are reported as ng/mL (as Hg). The liquid subsamples were processed by passing the desired quantity of sample through a 13 mm diameter syringe filter unit containing a 0.45 µM hydrophilic PTFE membrane into a premeasured quantity of DI water. The sample was mixed and further diluted in stages. Due to the high starting concentrations, the nominal serial dilution process used for all samples resulted in a total dilution factor of 34,500. A 0.1 mL aliquot of the final dilutions was pipetted into a sample boat that was preloaded with 0.5 mL of granular alumina to help retain the analyte and the boat was placed in the Milestone DMA-80 for analysis. The concentration in the liquid phase was calculated by dividing the mass of mercury (ng) in the aliquot by the volume of the aliquot and multiplying the result by the DF. The liquid phase results are reported as ng/mL as Hg. For microcosms where the methylmercury compound precipitated to form a solid phase, the gas concentrations and liquid concentrations represent the vapor pressure and solubility.

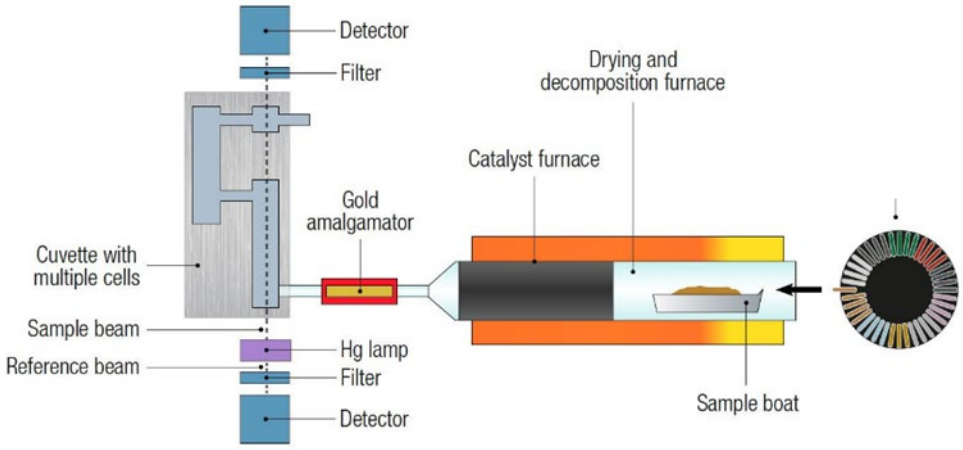

Figure 3-3. Generalized Diagram of Sparging Set-Up and Direct Mercury Analyzer (DMA-80)

Microcosms were prepared to provide for replicates. Logistically, this allowed for three to five conditions to be tested simultaneously. Thus, the work was completed in four campaigns (Table 3-2).

Table 3-2. Generalized Summary of Mercury Analysis Campaign Conditions.

Conditions	Notes
Campaign 1	
CH_3HgOH in DI water	
CH_3HgOH in NO_3 simulant	
CH_3HgOH in OH simulant	
Campaign 2	
CH_3HgOH + HCl (CH_3HgCl)	pH 11
CH_3HgOH + H_2SO_4 (CH_3HgSO_4)	
CH_3HgOH + NaOH	medium ionic strength
CH_3HgOH + NaOH	high ionic strength
Campaign 3	
CH_3HgOH + HCl (CH_3HgCl)	pH 7
CH_3HgOH + HCl (CH_3HgCl)	pH 4
CH_3HgOH + formic acid	CH_3Hg formate
CH_3HgOH + glycolic acid	CH_3Hg glycolate
Campaign 4	
Various additional replicates and confirmation runs	

This sampling was typically performed in triplicate (two to five microcosms per condition) with three to five conditions run in each campaign. Repeated sampling was done when necessary. Over 200 individual sample results were generated during the study.

4.0 Results and Discussion

The results for the microcosms are presented below for each of three topical areas: 1) Henry's Law, 2) vapor pressure and solubility, and 3) observed reaction of methylmercury with formic acid resulting in dimethylmercury. For the first two topical areas, the raw data are presented in graphical form, along with graphical and tabular projections of the expected values based on empirical and thermodynamic relationships. For Henry's Law, vapor pressure, and solubility, the temperature predictions are described using the Van't Hoff Equation, the Antoine Equation, and the enthalpy of solution, respectively. In each section, the data generated in this study are initially checked and validated against the available literature; generally, at 20 to 25 °C for methylmercury chloride and/or methylmercury hydroxide.

4.1 Henry's Law (Gas-Liquid Partitioning)

This research was primarily intended to provide parameters for SRR scientists and engineers to make flowsheet and design calculations. Henry's Law is a principal physical/chemical parameter that will assist in understanding the partitioning and the general behavior of methylmercury throughout the LWS.

There are limited data available in the literature for H' of methylmercury (Iverfeldt and Persson, 1985; Mueleman et al., 1993; EPA, 2017; Talmi and Messmer, 1975; and Brossett and Lord, 1995). Figure 4-1 summarizes the available literature and the results from this study, along with the range of values from the literature. As shown, the measured H' values at 20 to 22 °C for methylmercury chloride and hydroxide in this study are close to the median values from the literature at 20 °C to 25 °C. All of the H' data for CH_3HgCl cluster tightly around the median value of 2.2×10^{-5} at these "ambient" temperatures. As demonstrated in the more detailed information below, the relatively tight clustering of data for CH_3HgCl compared to CH_3HgOH may result, in part, from the higher concentrations of CH_3HgCl in the gas phase and from the relative insensitivity of measured H' for CH_3HgCl to changes in ionic strength and temperature. Notably, in setting up their headspace microcosm for CH_3HgOH, Mueleman et al. (1993) used a liquid phase with high ionic strength which resulted in a measured H' that was significantly higher and not consistent with the other references in the literature. Based on this method difference, the value for Meuleman was not included in the median. The close correspondence of the results from this study to the literature provide an initial validation of the straightforward headspace paradigm developed by SRNL, as well as the analytical protocols. These protocols include reagent preparation, gas and liquid subsampling, mercury trapping for gas samples, filtering and serial dilutions for liquid samples, and mercury quantification using the Milestone DMA-80.

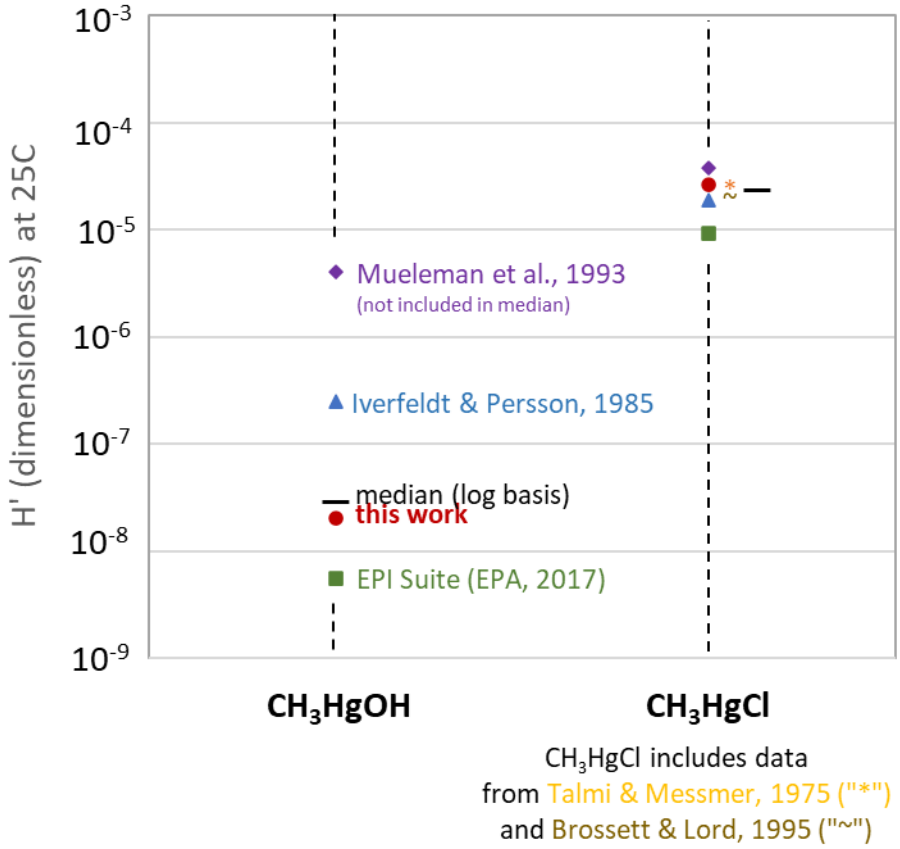

Figure 4-1. Comparison of Henry's Law Coefficients for Measured MeHgOH and MeHgCl to Available Literature (at 20 to 25 °C)

For each of the compounds and conditions, the raw data and the Van't Hoff temperature projections are presented in a composite figure consisting of a graphic (Van't Hoff plot) and a table of projected H' as a function of temperature from 0 to 100 °C. The plots were constructed in the traditional format (Figure 4-2) using the inverse absolute temperature on the x axis (in units of 1/°K) and the natural log of the H' on the y axis.

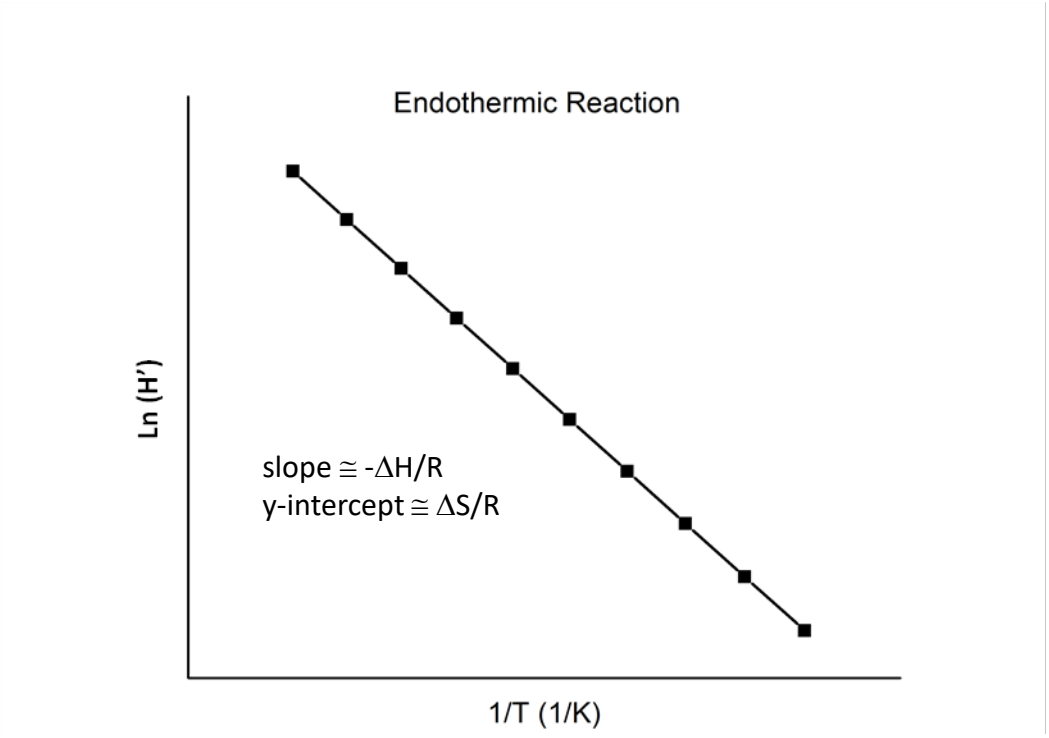

Figure 4-2. Standard Format Van't Hoff Plot for an Endothermic Process and the Interpretation of the Slope and Intercept

The data for this study were matched to the Van't Hoff equation by best fit. The resulting Van't Hoff plots show the raw data as points, the best estimate projection line as a solid line, and curved lines that bound the lower and upper 95 % confidence intervals on the estimated relationship. The Van't Hoff equation provided reasonable estimates of the relationship between H' and temperature. The order of the data plots in the report is as follows:

Figure 4-3 – CH_3HgOH in 0.02 M NaOH
Figure 4-4 – CH_3Hg+ in NO_3 Simulant
Figure 4-5 – CH_3Hg+ in OH Simulant
Figure 4-6 – CH_3HgSO_4 in Water (pH 7)
Figure 4-7 – CH_3HgCl in Water (pH 11)
Figure 4-8 – CH_3HgCl in Water (pH 7)
Figure 4-9 – CH_3HgCl in Water (pH 4)
Figure 4-10 – CH3Hg Glycolate in Water (pH 7)
Figure 4-11 – CH_3HgOH in 0.51 M NaOH
Figure 4-12 – CH_3HgOH in 1.51 M NaOH

The H' for CH_3HgOH in dilute solution (approximately 0.02 M OH) was relatively low; nominally 2.22 x 10^{-8} at 25 °C. As shown in Figure 4-3, the H' for CH_3HgOH in dilute solution exhibited a strong function of temperature; ranging over approximately 5 orders of magnitude from 0 °C to 100 °C. For example, H' for CH_3HgOH under those conditions increased from 3.87 x 10^{-10} at 0 °C up to 6.36 x 10^{-5} at 100 °C. As expected from the literature, the methylmercury compound with the highest H' at ambient temperature was CH_3HgCl (nominally 2 x 10^{-5}). Compared to CH_3HgOH, increasing temperature had a smaller impact on the H' of CH_3HgCl as seen in the flatter slope in the Van't Hoff plots (Figure 4-7, Figure 4-8 and Figure 4-9). The H' values for CH_3HgCl increased by about 3.5 orders of magnitude as temperature increased from 0 °C to 100 °C.

The H' values for CH_3HgSO_4, CH_3Hg glycolate, and CH_3Hg^+ in the blended simulants (Figure 4-4, Figure 4-5, and Figure 4-6, respectively) were intermediate between CH_3HgOH and CH_3HgCl. Similarly, the relationship of H' to temperature for CH_3HgSO_4 and for CH_3Hg^+ in the blended simulants was intermediate between CH_3HgOH and CH_3HgCl.

As shown in Figure 4-7, Figure 4-8, and Figure 4-9, the H' for CH_3HgCl was not a strong function of pH. The H' values were similar within experimental error for all of the tested pHs.

Conversely, ionic strength had a strong impact on the H' for CH_3HgOH over the entire temperature range of 0 °C to 100 °C. Figure 4-3, Figure 4-11, and Figure 4-12 document the changes in H' for CH_3HgOH as the hydroxide was increased from 0.02 M to 0.51 M to 1.51 M. Over this range, the H' for CH_3HgOH increased by one or two orders of magnitude. Figure 4-13 shows how ionic strength and a "salting out effect" impacted H' for selected temperatures. Importantly, as ionic strength increased, the H' values for CH_3HgOH approached the values that were measured in the simulants at the same temperatures. This observation supports consideration of a simplified application of the study results to LWS conditions. The robustness of the data and approach are explored in more detail below.

No H' data were generated for the formate microcosm because the CH_3Hg^+ reacted with formate and resulted in the synthesis of a volatile reaction product. This is discussed in more detail in a separate section of the report.

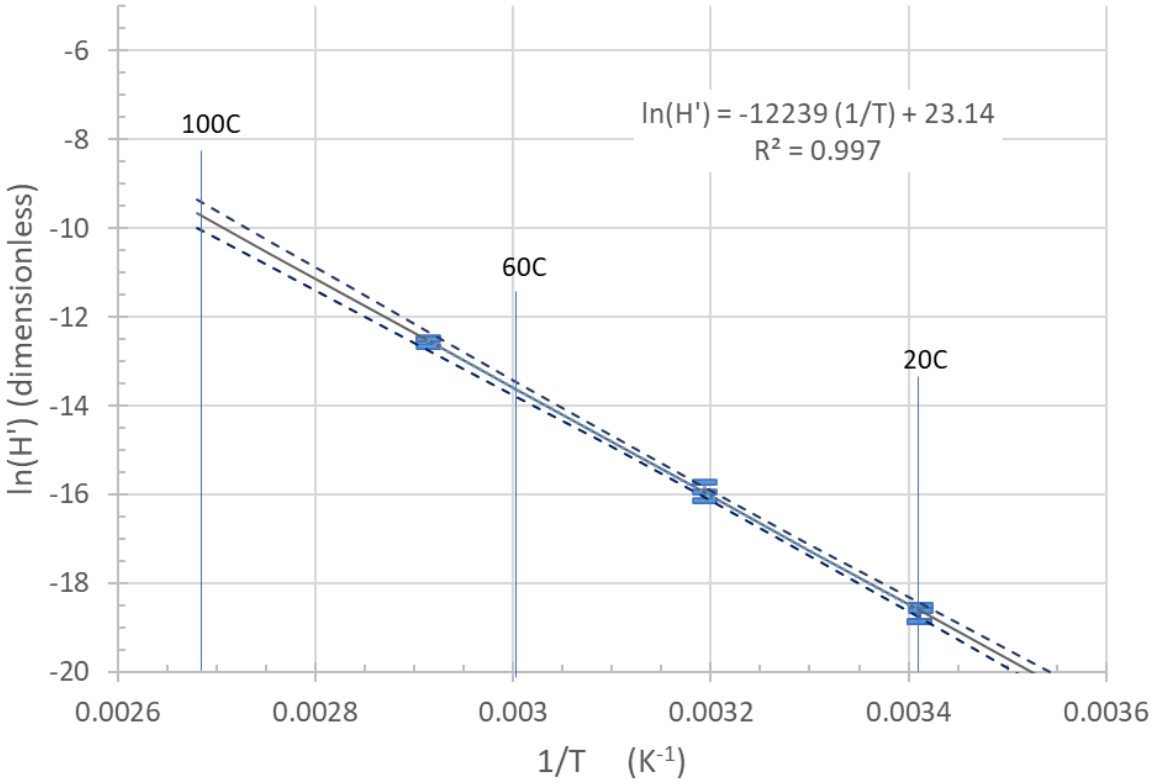

Temperature (°C)	H'	95% confidence range		
0	3.87×10^{-10}	2.90×10^{-10}	to	5.18×10^{-10}
10	1.89×10^{-9}	1.51×10^{-9}	to	2.36×10^{-9}
20	8.24×10^{-9}	6.95×10^{-9}	to	9.77×10^{-9}
30	3.27×10^{-8}	2.86×10^{-8}	to	3.72×10^{-8}
40	1.19×10^{-7}	1.05×10^{-7}	to	1.33×10^{-7}
50	3.97×10^{-7}	3.48×10^{-7}	to	4.53×10^{-7}
60	1.24×10^{-6}	1.05×10^{-6}	to	1.46×10^{-6}
70	3.61×10^{-6}	2.96×10^{-6}	to	4.41×10^{-6}
80	9.92×10^{-6}	7.80×10^{-6}	to	1.26×10^{-5}
90	2.58×10^{-5}	1.95×10^{-5}	to	3.41×10^{-5}
100	6.36×10^{-5}	4.62×10^{-5}	to	8.74×10^{-5}

Figure 4-3. Van't Hoff Plot for CH_3HgOH in Water (Approximately 0.02 M OH^-)

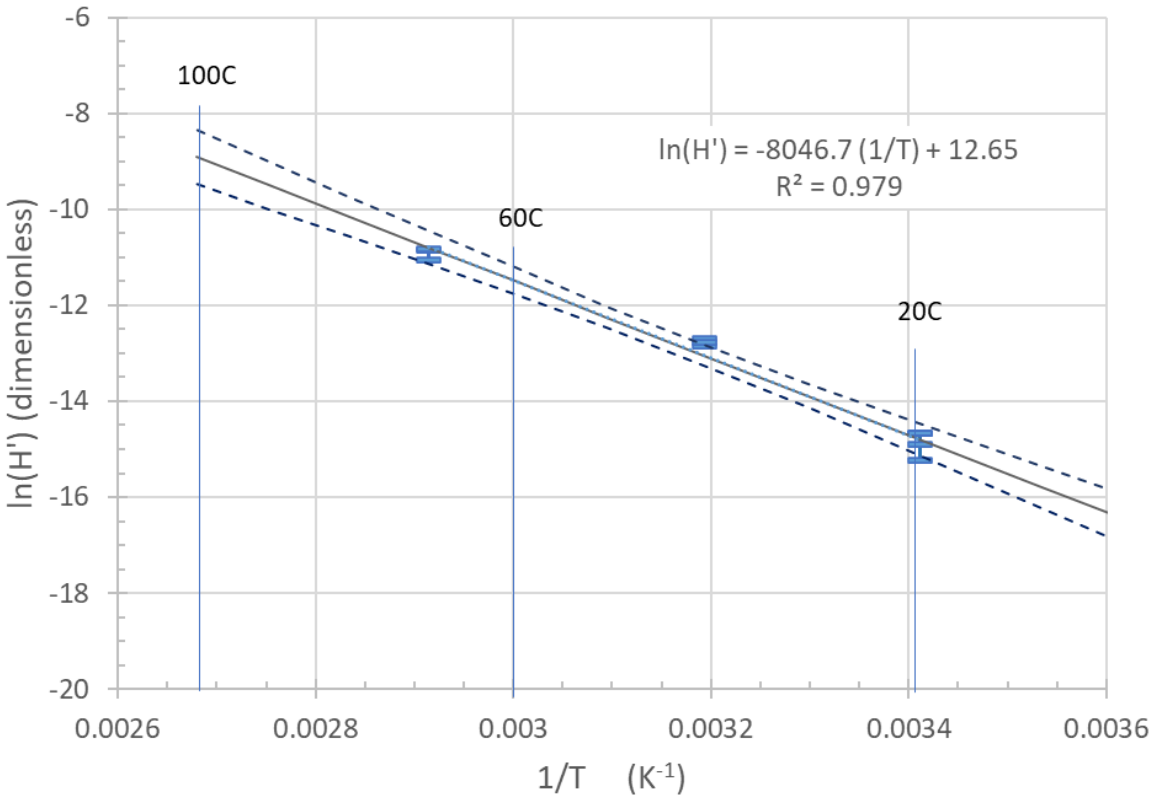

Temperature (°C)	H'	95% confidence range		
0	5.03×10^{-8}	2.89×10^{-8}	to	$8.76\ 10^{-8}$
10	1.42×10^{-7}	9.23×10^{-8}	to	2.19×10^{-7}
20	3.75×10^{-7}	2.70×10^{-7}	to	5.21×10^{-7}
30	9.28×10^{-7}	7.22×10^{-7}	to	1.19×10^{-6}
40	2.17×10^{-6}	1.75×10^{-6}	to	2.68×10^{-6}
50	4.80×10^{-6}	3.82×10^{-6}	to	6.03×10^{-6}
60	1.01×10^{-5}	7.66×10^{-6}	to	1.34×10^{-5}
70	2.05×10^{-5}	1.45×10^{-5}	to	2.89×10^{-5}
80	3.98×10^{-5}	2.62×10^{-5}	to	6.04×10^{-5}
90	7.45×10^{-5}	4.57×10^{-5}	to	1.22×10^{-4}
100	1.35×10^{-4}	7.70×10^{-5}	to	2.36×10^{-4}

Figure 4-4. Van't Hoff Plot for CH_3Hg^+ in NO_3 Simulant

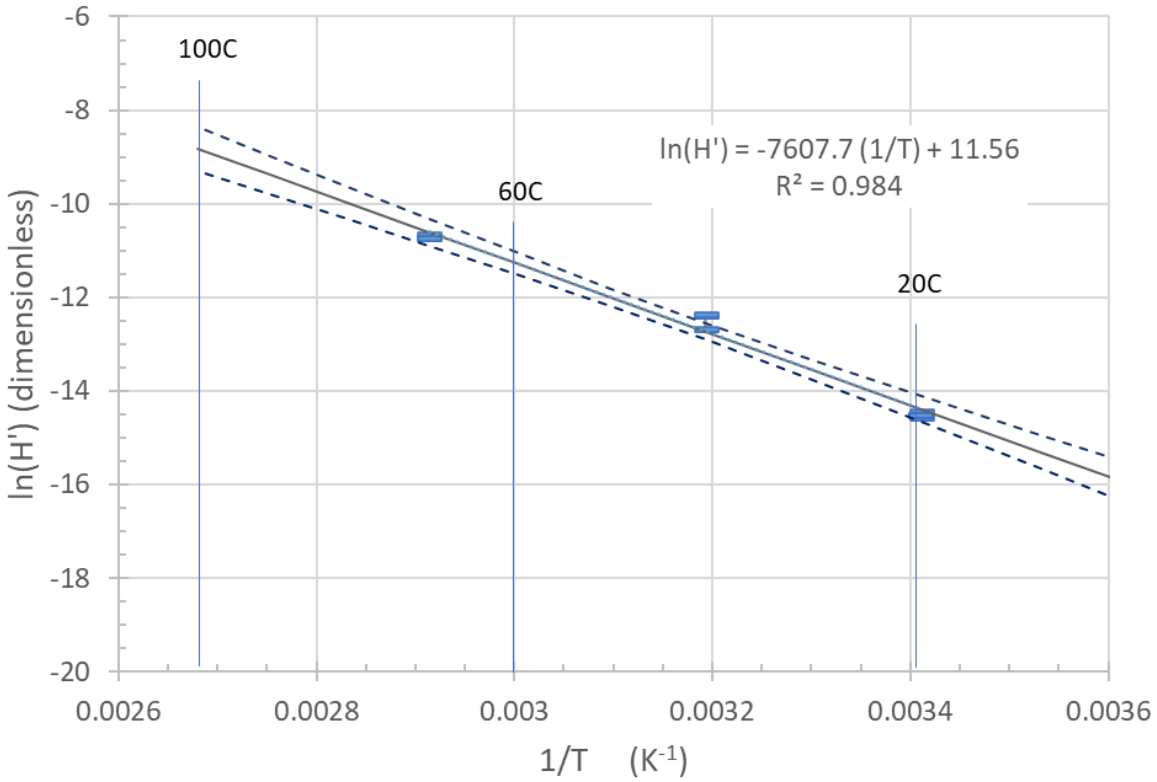

Temperature (°C)	H'	95% confidence range		
0	8.44×10^{-8}	5.32×10^{-8}	to	1.34×10^{-7}
10	2.26×10^{-7}	1.57×10^{-7}	to	3.24×10^{-7}
20	5.65×10^{-7}	4.29×10^{-7}	to	7.42×10^{-7}
30	1.33×10^{-6}	1.08×10^{-6}	to	1.64×10^{-6}
40	2.96×10^{-6}	2.48×10^{-6}	to	3.54×10^{-6}
50	6.28×10^{-6}	5.19×10^{-6}	to	7.60×10^{-6}
60	1.27×10^{-5}	1.01×10^{-5}	to	1.61×10^{-5}
70	2.48×10^{-5}	1.86×10^{-5}	to	3.30×10^{-5}
80	4.64×10^{-5}	3.28×10^{-5}	to	6.57×10^{-5}
90	8.40×10^{-5}	5.59×10^{-5}	to	1.26×10^{-4}
100	1.47×10^{-4}	9.24×10^{-5}	to	2.35×10^{-4}

Figure 4-5. Van't Hoff Plot for CH_3Hg^+ in OH Simulant

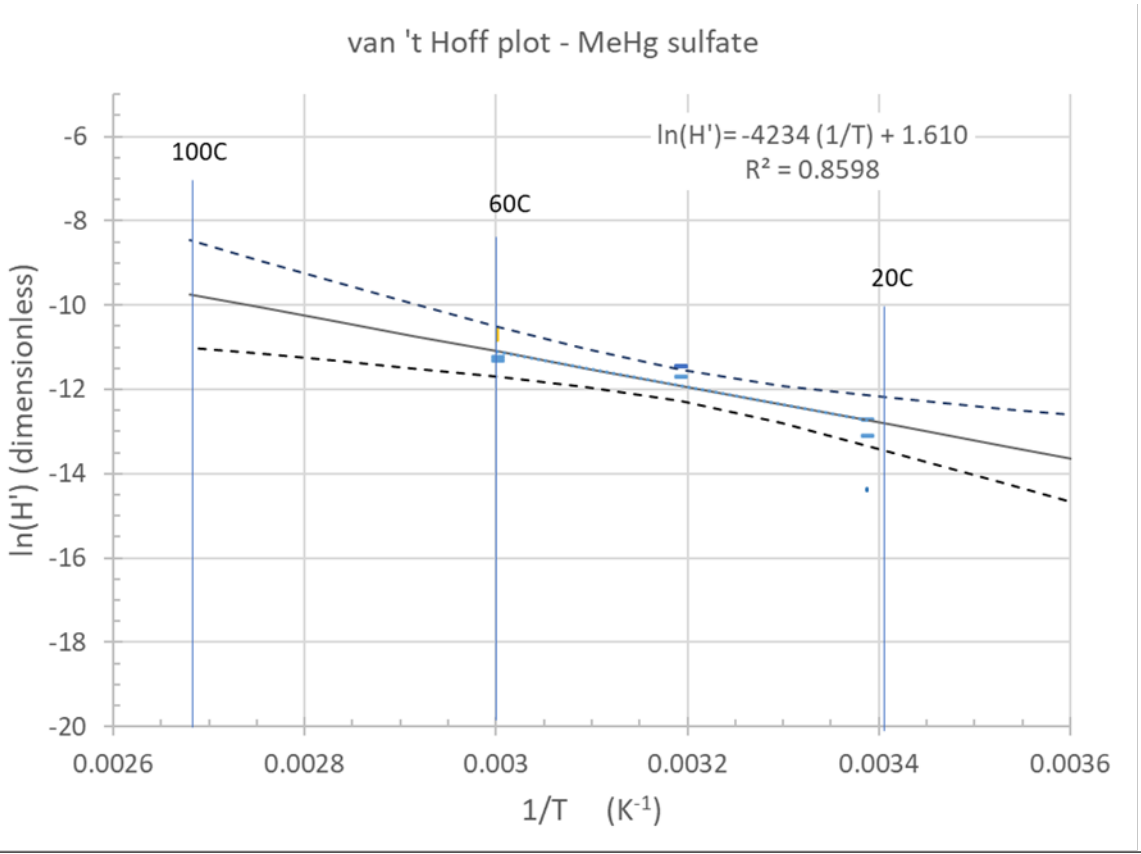

Temperature (°C)	H'	95% Confidence range		
0	9.27×10^{-7}	2.88×10^{-7}	to	2.98×10^{-6}
10	1.60×10^{-6}	6.62×10^{-7}	to	3.88×10^{-6}
20	2.67×10^{-6}	1.41×10^{-6}	to	5.04×10^{-6}
30	4.30×10^{-6}	2.74×10^{-6}	to	6.73×10^{-6}
40	6.71×10^{-6}	4.62×10^{-6}	to	9.76×10^{-6}
50	1.02×10^{-5}	6.55×10^{-6}	to	1.59×10^{-5}
60	1.51×10^{-5}	8.37×10^{-6}	to	2.73×10^{-5}
70	2.19×10^{-5}	1.02×10^{-5}	to	4.70×10^{-5}
80	3.10×10^{-5}	1.21×10^{-5}	to	7.94×10^{-5}
90	4.32×10^{-5}	1.42×10^{-5}	to	1.31×10^{-4}
100	5.90×10^{-5}	1.65×10^{-5}	to	2.12×10^{-4}

Figure 4-6. Van't Hoff Plot for CH_3HgSO_4 in Water (pH 7)

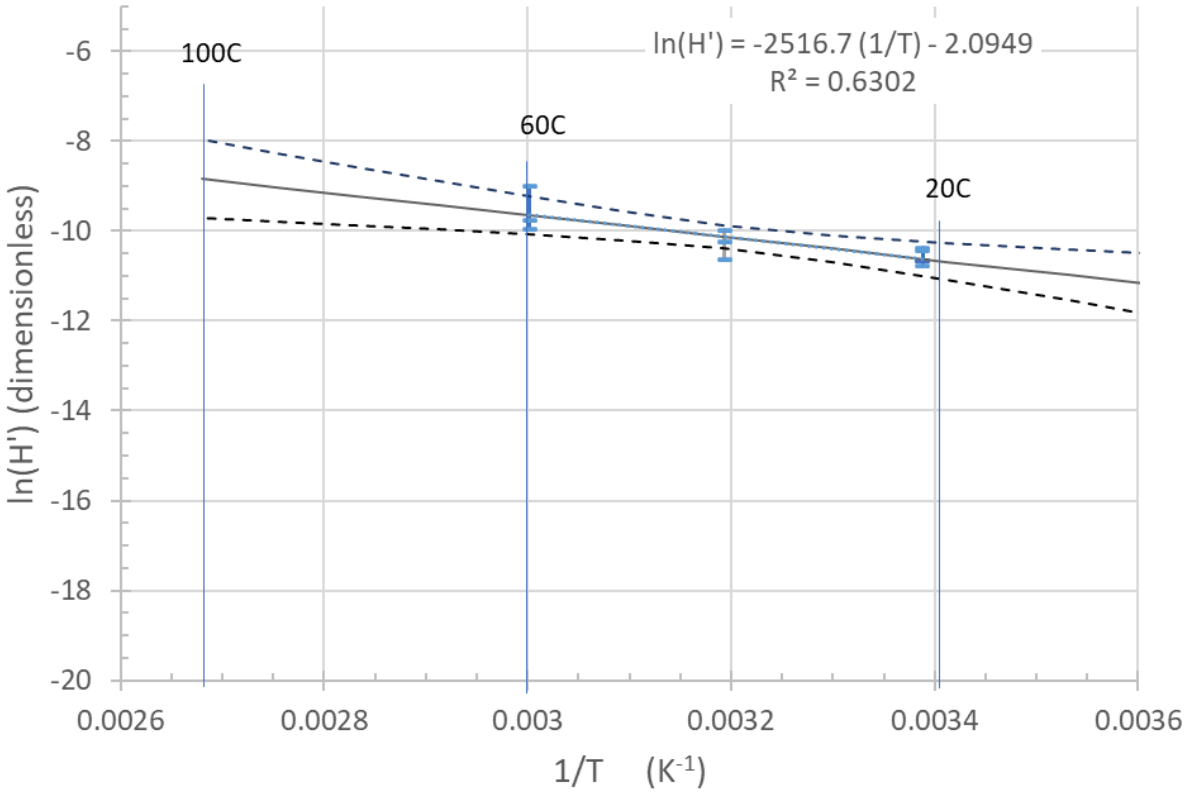

Temperature (°C)	H'	95% confidence range		
0	1.22×10^{-5}	5.79×10^{-6}	to	2.59×10^{-5}
10	1.70×10^{-5}	9.73×10^{-6}	to	2.98×10^{-5}
20	2.30×10^{-5}	1.54×10^{-5}	to	3.43×10^{-5}
30	3.06×10^{-5}	2.30×10^{-5}	to	4.07×10^{-5}
40	3.97×10^{-5}	3.07×10^{-5}	to	5.12×10^{-5}
50	5.09×10^{-5}	3.72×10^{-5}	to	6.98×10^{-5}
60	6.44×10^{-5}	4.23×10^{-5}	to	9.81×10^{-5}
70	8.07×10^{-5}	4.73×10^{-5}	to	1.38×10^{-4}
80	9.90×10^{-5}	5.17×10^{-5}	to	1.90×10^{-4}
90	1.20×10^{-4}	5.60×10^{-5}	to	2.59×10^{-4}
100	1.45×10^{-4}	6.01×10^{-5}	to	3.49×10^{-4}

Figure 4-7. Van't Hoff Plot for CH_3HgCl in Water (pH 11)

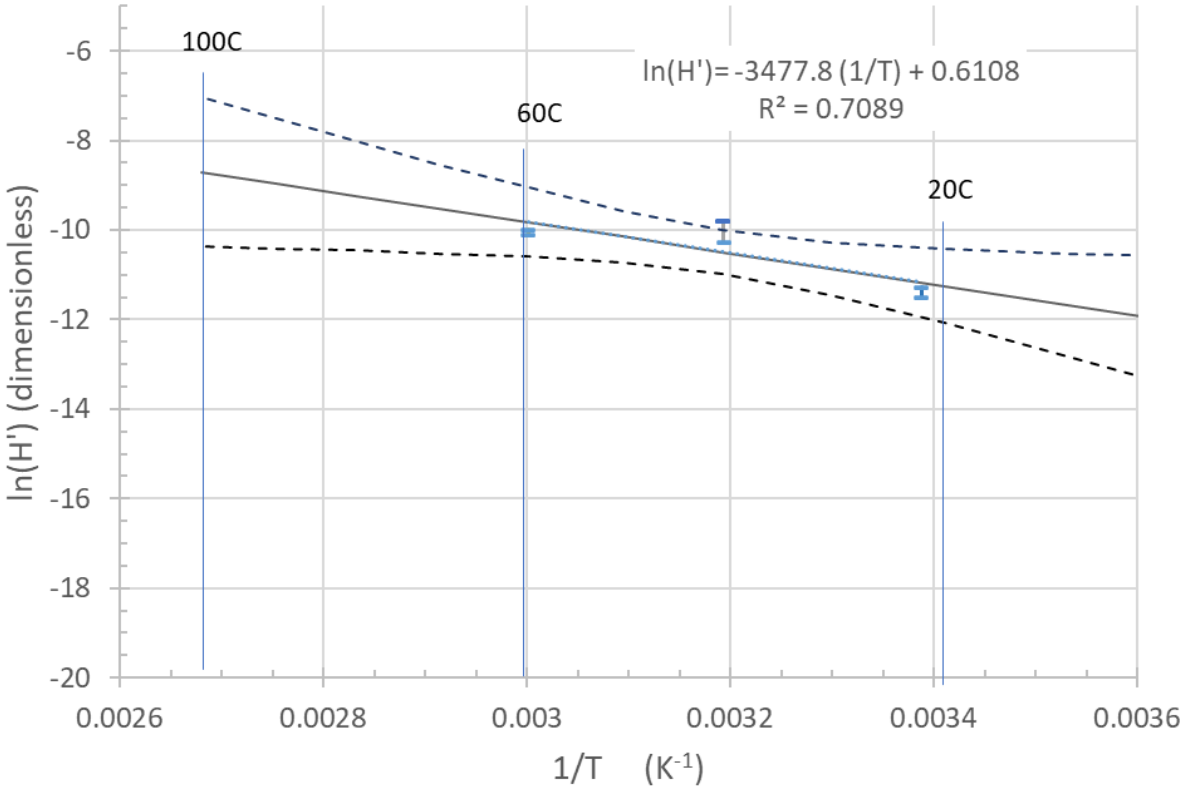

Temperature (˚C)	H'	95% confidence range		
0	5.42×10^{-6}	1.18×10^{-6}	to	2.49×10^{-5}
10	8.55×10^{-6}	2.71×10^{-6}	to	2.70×10^{-5}
20	1.30×10^{-5}	5.67×10^{-6}	to	2.98×10^{-5}
30	1.91×10^{-5}	1.06×10^{-5}	to	3.43×10^{-5}
40	2.77×10^{-5}	1.70×10^{-5}	to	4.49×10^{-5}
50	3.91×10^{-5}	2.19×10^{-5}	to	6.98×10^{-5}
60	5.38×10^{-5}	2.49×10^{-5}	to	1.16×10^{-4}
70	7.30×10^{-5}	2.70×10^{-5}	to	1.97×10^{-4}
80	9.76×10^{-5}	2.87×10^{-5}	to	3.32×10^{-4}
90	1.28×10^{-4}	3.01×10^{-5}	to	5.42×10^{-4}
100	1.66×10^{-4}	3.14×10^{-5}	to	8.76×10^{-4}

Figure 4-8. Van't Hoff Plot for CH_3HgCl in Water (pH 7)

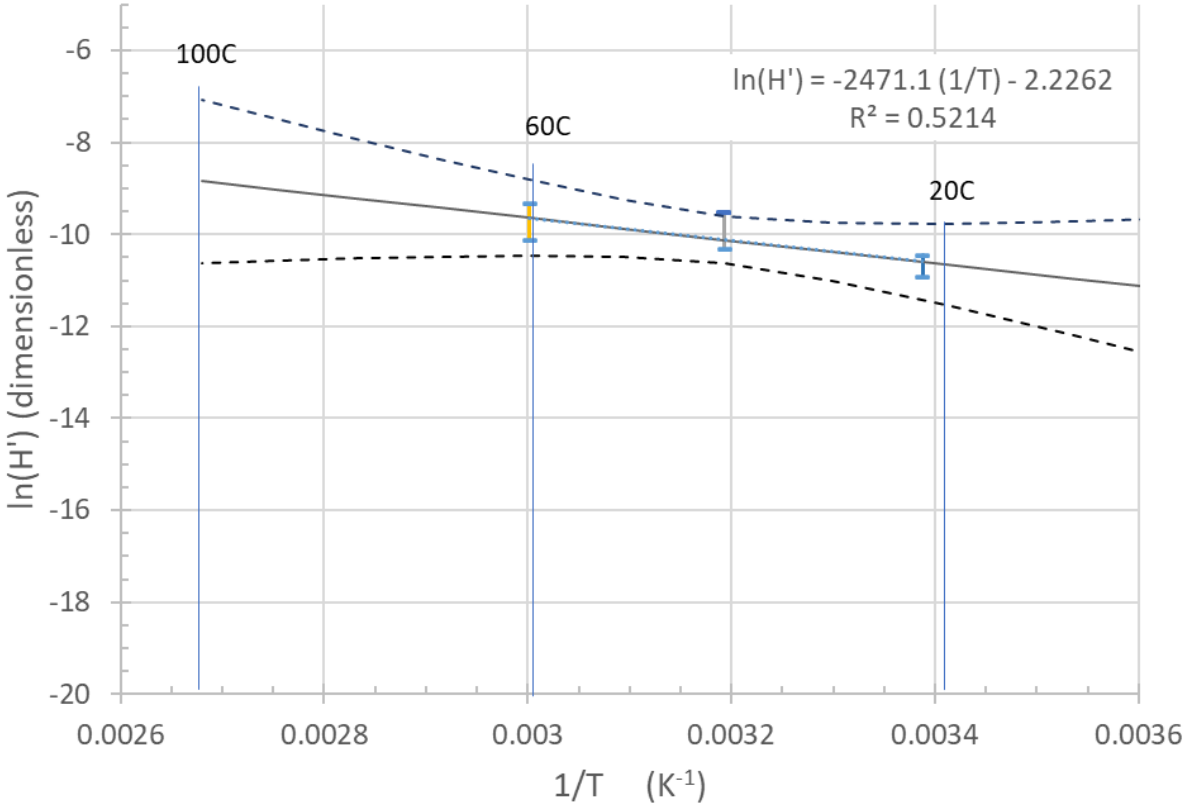

Temperature (°C)	H'	95% confidence range		
0	1.27×10^{-5}	2.52×10^{-6}	to	6.44×10^{-5}
10	1.75×10^{-5}	5.13×10^{-6}	to	5.95×10^{-5}
20	2.36×10^{-5}	9.73×10^{-6}	to	5.71×10^{-5}
30	3.10×10^{-5}	1.67×10^{-5}	to	5.77×10^{-5}
40	4.03×10^{-5}	2.39×10^{-5}	to	6.77×10^{-5}
50	5.14×10^{-5}	2.78×10^{-5}	to	9.52×10^{-5}
60	6.51×10^{-5}	2.87×10^{-5}	to	1.48×10^{-4}
70	8.07×10^{-5}	2.81×10^{-5}	to	2.32×10^{-4}
80	9.90×10^{-5}	2.70×10^{-5}	to	3.63×10^{-4}
90	1.20×10^{-4}	2.57×10^{-5}	to	5.59×10^{-4}
100	1.43×10^{-4}	2.44×10^{-5}	to	8.42×10^{-4}

Figure 4-9. Van't Hoff Plot for CH_3HgCl in Water (pH 4)

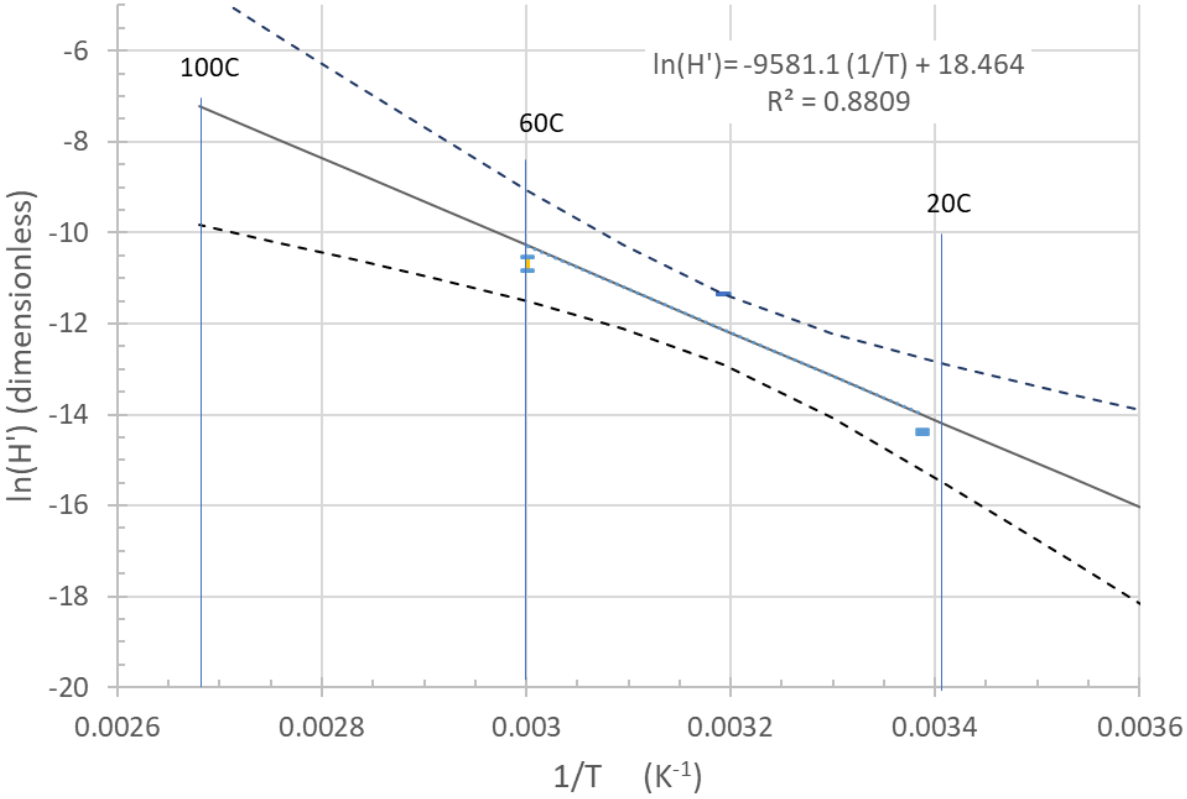

Temperature (˚C)	H'	95% confidence range		
0	6.11×10^{-8}	5.49×10^{-9}	to	6.81×10^{-7}
10	2.11×10^{-7}	3.42×10^{-8}	to	1.30×10^{-6}
20	6.67×10^{-7}	1.80×10^{-7}	to	2.47×10^{-6}
30	1.96×10^{-6}	7.75×10^{-7}	to	4.93×10^{-6}
40	5.40×10^{-6}	2.50×10^{-6}	to	1.17×10^{-5}
50	1.39×10^{-5}	5.56×10^{-6}	to	3.47×10^{-5}
60	3.38×10^{-5}	1.00×10^{-5}	to	1.14×10^{-4}
70	7.83×10^{-5}	1.62×10^{-5}	to	3.78×10^{-4}
80	1.73×10^{-4}	2.49×10^{-5}	to	1.19×10^{-3}
90	3.63×10^{-4}	3.68×10^{-5}	to	3.59×10^{-3}
100	7.39×10^{-4}	5.33×10^{-5}	to	1.03×10^{-2}

Figure 4-10. Van't Hoff Plot for CH_3Hg Glycolate

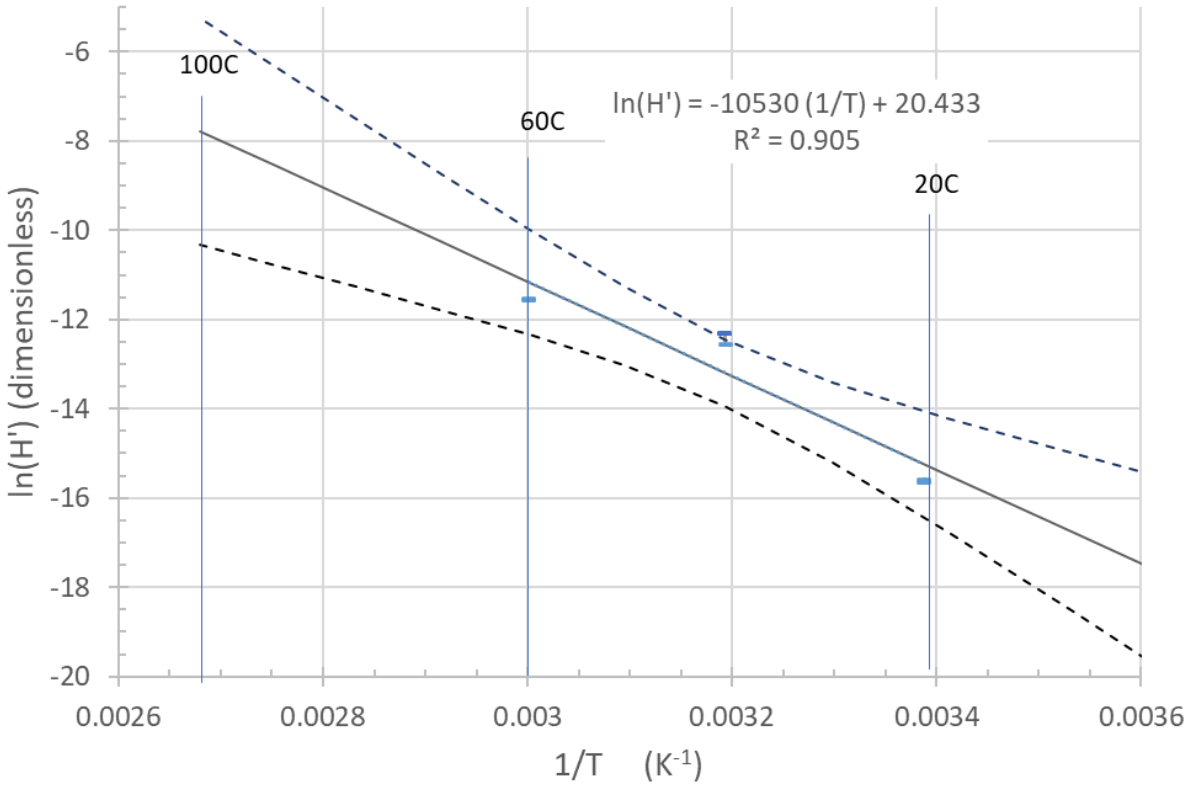

Temperature (°C)	H'	95% confidence range		
0	1.36×10^{-8}	1.31×10^{-9}	to	1.40×10^{-7}
10	5.29×10^{-8}	9.05×10^{-9}	to	3.09×10^{-7}
20	1.88×10^{-7}	5.26×10^{-8}	to	6.67×10^{-7}
30	6.15×10^{-7}	2.50×10^{-7}	to	1.50×10^{-6}
40	1.86×10^{-6}	8.83×10^{-7}	to	3.92×10^{-6}
50	5.28×10^{-6}	2.17×10^{-6}	to	1.27×10^{-5}
60	1.40×10^{-5}	4.33×10^{-6}	to	4.59×10^{-5}
70	3.53×10^{-5}	7.66×10^{-6}	to	1.62×10^{-4}
80	8.41×10^{-5}	1.29×10^{-5}	to	5.48×10^{-4}
90	1.91×10^{-4}	2.08×10^{-5}	to	1.75×10^{-3}
100	4.16×10^{-4}	3.26×10^{-5}	to	5.30×10^{-3}

Figure 4-11. Van't Hoff Plot for CH_3HgOH in 0.51 M NaOH

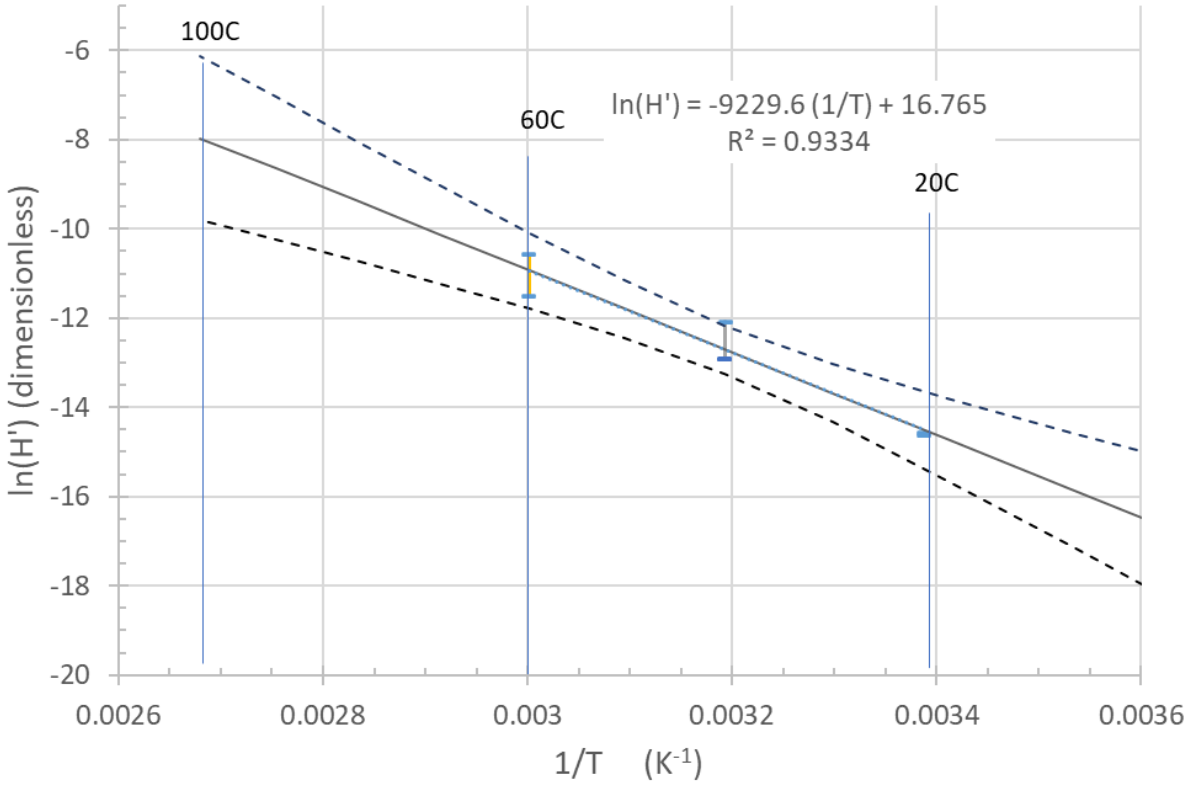

Temperature (°C)	H'	95% confidence range		
0	4.04×10^{-8}	7.49×10^{-9}	to	2.18×10^{-7}
10	1.33×10^{-7}	3.71×10^{-8}	to	4.75×10^{-7}
20	4.05×10^{-7}	1.61×10^{-7}	to	1.02×10^{-6}
30	1.14×10^{-6}	5.98×10^{-7}	to	2.19×10^{-6}
40	3.03×10^{-6}	1.76×10^{-6}	to	5.18×10^{-6}
50	7.53×10^{-6}	3.96×10^{-6}	to	1.42×10^{-5}
60	1.78×10^{-5}	7.58×10^{-6}	to	4.15×10^{-5}
70	3.98×10^{-5}	1.33×10^{-5}	to	1.20×10^{-4}
80	8.52×10^{-5}	2.21×10^{-5}	to	3.29×10^{-4}
90	1.75×10^{-4}	3.54×10^{-5}	to	8.67×10^{-4}
100	3.46×10^{-4}	5.49×10^{-5}	to	2.18×10^{-3}

Figure 4-12. Van't Hoff Plot for CH_3HgOH in 1.51 M NaOH

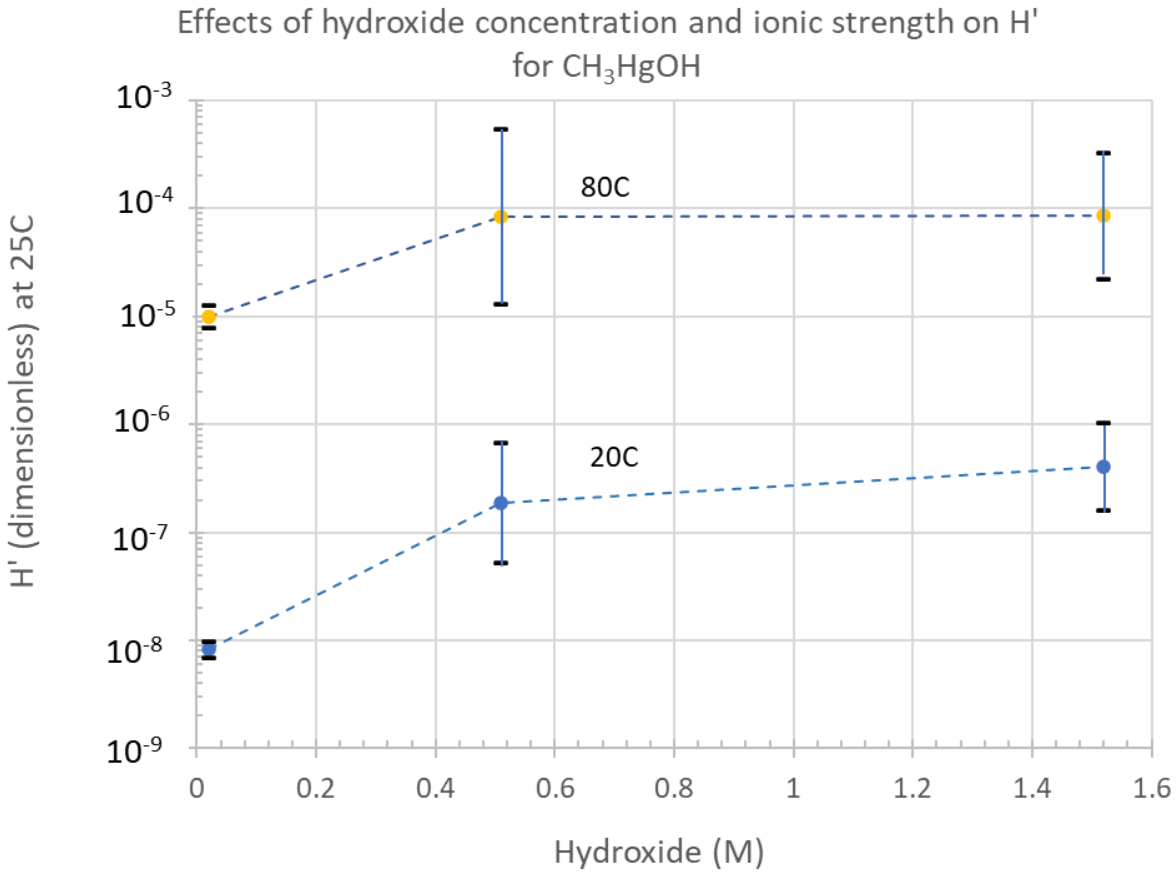

Figure 4-13. Effects of Hydroxide Concentration and Ionic Strength on H' for CH_3HgOH

Figure 4-14 through Figure 4-18 summarize the H' information for the various tested compounds and conditions over a range of temperatures from 0 C to 100 C:

Figure 4-14 – H' for all compounds and conditions at 20 °C
Figure 4-15 – H' for all compounds and conditions at 40 °C
Figure 4-16 – H' for all compounds and conditions at 60 °C
Figure 4-17 – H' for all compounds and conditions at 80 °C
Figure 4-18 – H' for all compounds and conditions at 100 °C

As expected, increasing temperature results in increasing H' for all compounds. In these summary graphs, CH_3HgOH in dilute solution has the lowest H' and CH_3HgCl generally has the highest H'. The other compounds and conditions are bound by these end members. Several observations provide significant context that augment and annotate these broad trends. First, as ionic strength increases to high levels, the measured H' for pure CH_3HgOH in a simple solution containing only CH_3HgOH, Na^+, and OH^- closely aligns to the measured H' in both LWS simulants. Second, the H' values for methylmercury sulfate and glycolate (i.e., the tested compounds other than chloride) were similar to those of CH_3HgOH in the high ionic strength solution and to the simulants. These results suggest that CH_3Hg^+ partitioning in typical high ionic strength and high hydroxide conditions are likely controlled by the dominant CH_3HgOH species and/or by other non-chloride species with a similar H' ratio between vapor pressure and solubility. Since the chloride ion is procedurally avoided to minimize corrosion in the LWS, these results suggest that reasonable scoping values for H' can be developed for application throughout the LWS for all temperatures. Because of the different slopes in the Van't Hoff plots, the H' values at higher temperatures (e.g., 80°C and 100°C) trend toward similar values for all compounds; including CH_3HgCl. This further corroborates the potential robustness of scoping values for H' applied to LWS conditions at higher temperatures.

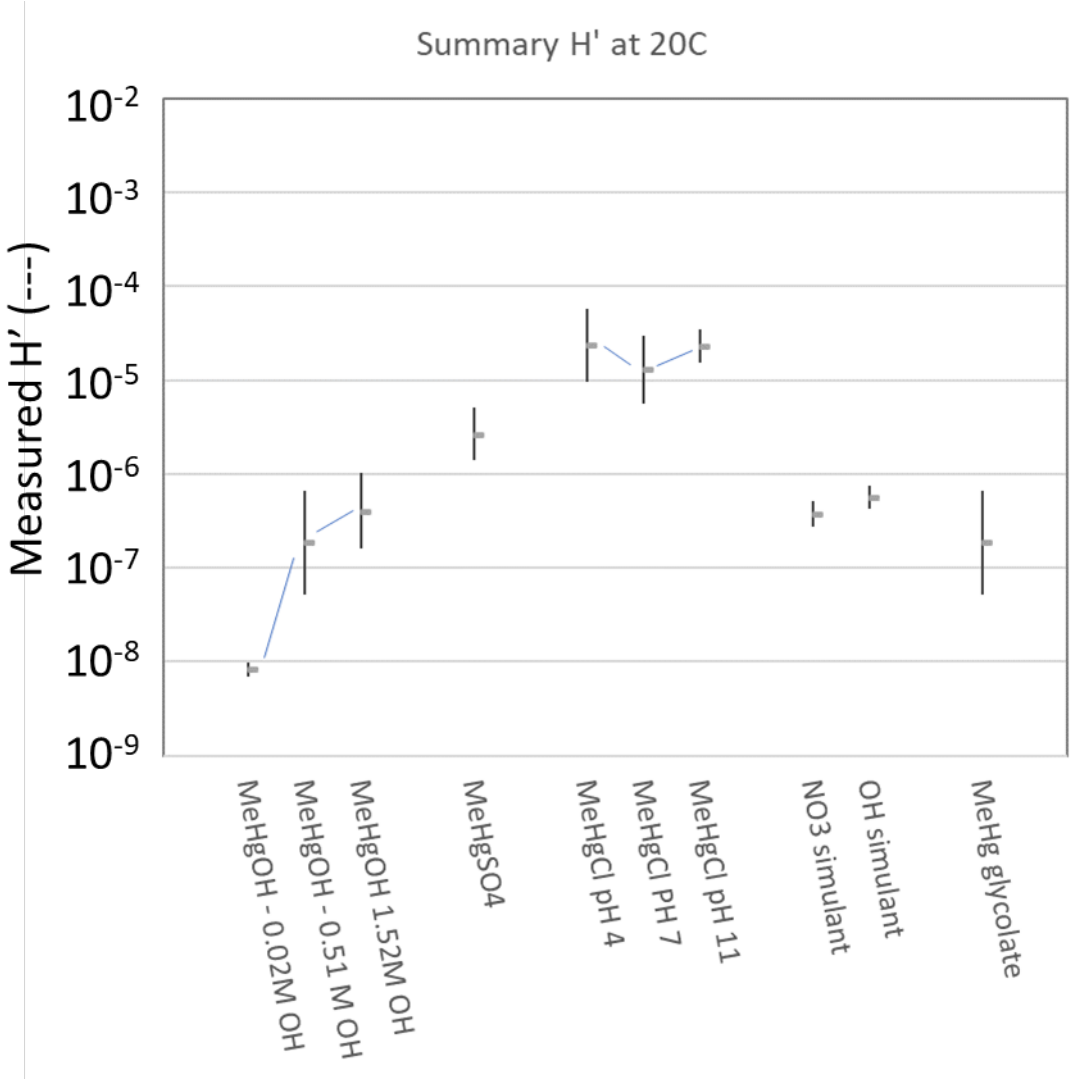

Figure 4-14. Summary H' at 20 °C

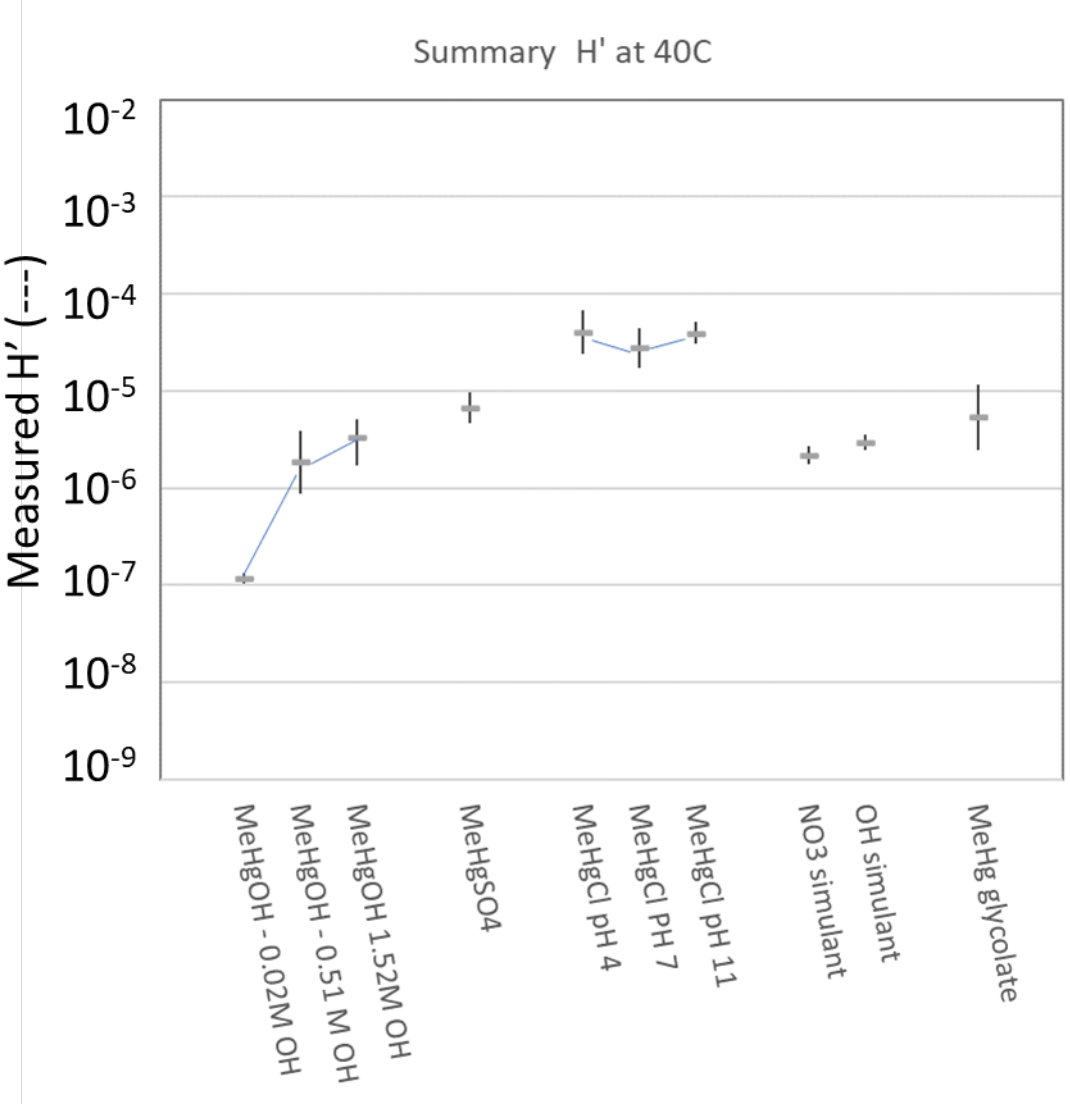

Figure 4-15. Summary H' at 40 °C

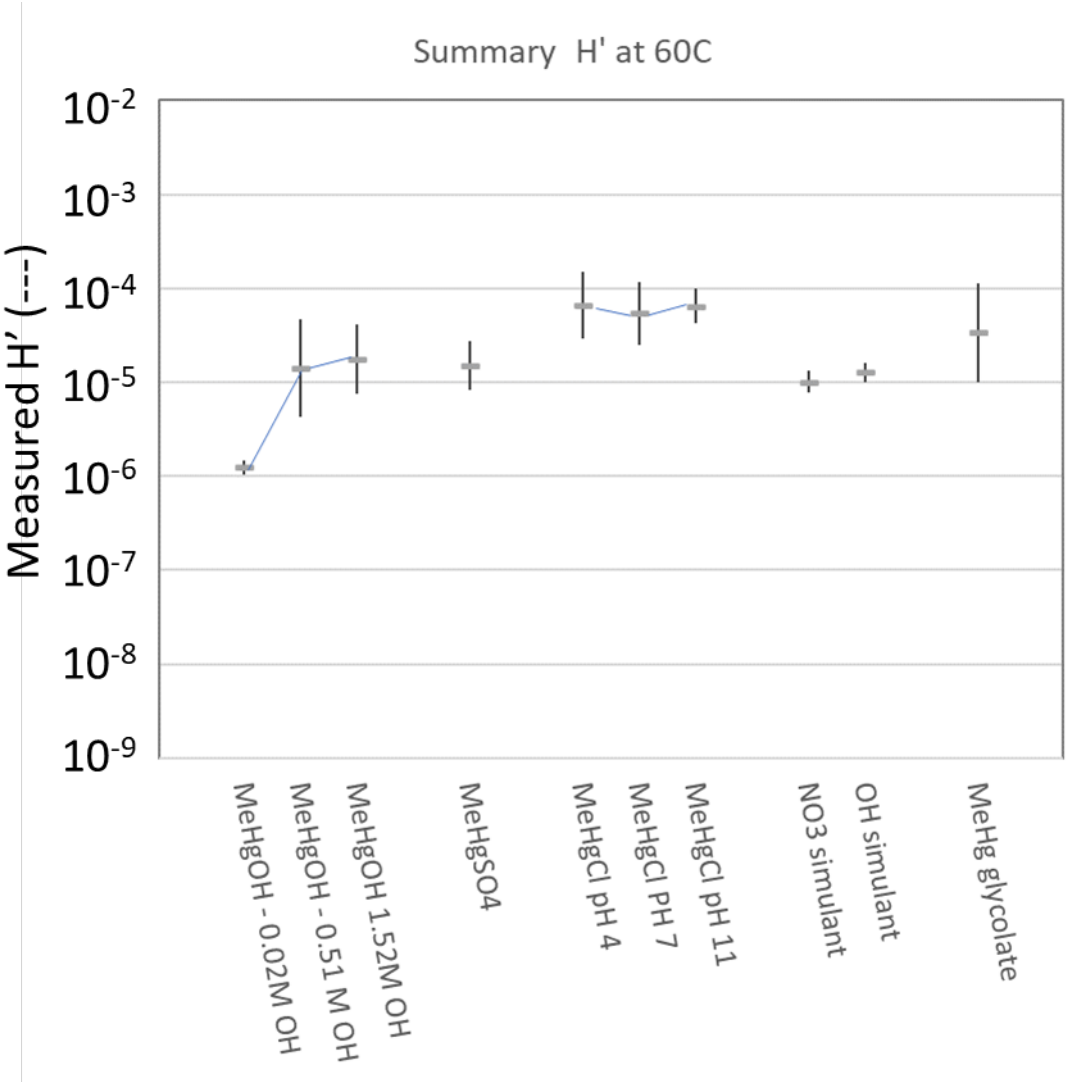

Figure 4-16. Summary H' at 60 °C

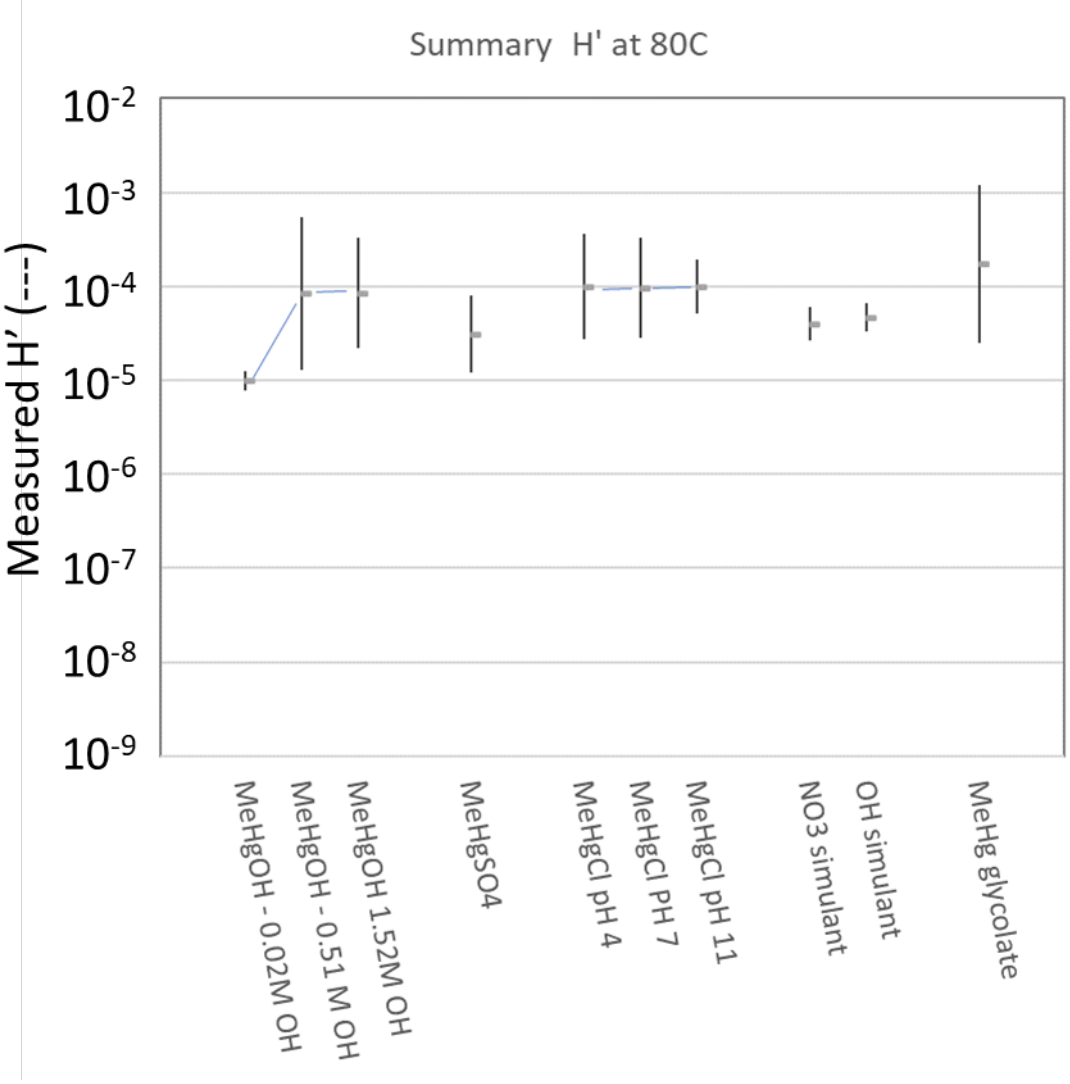

Figure 4-17. Summary H' at 80 °C

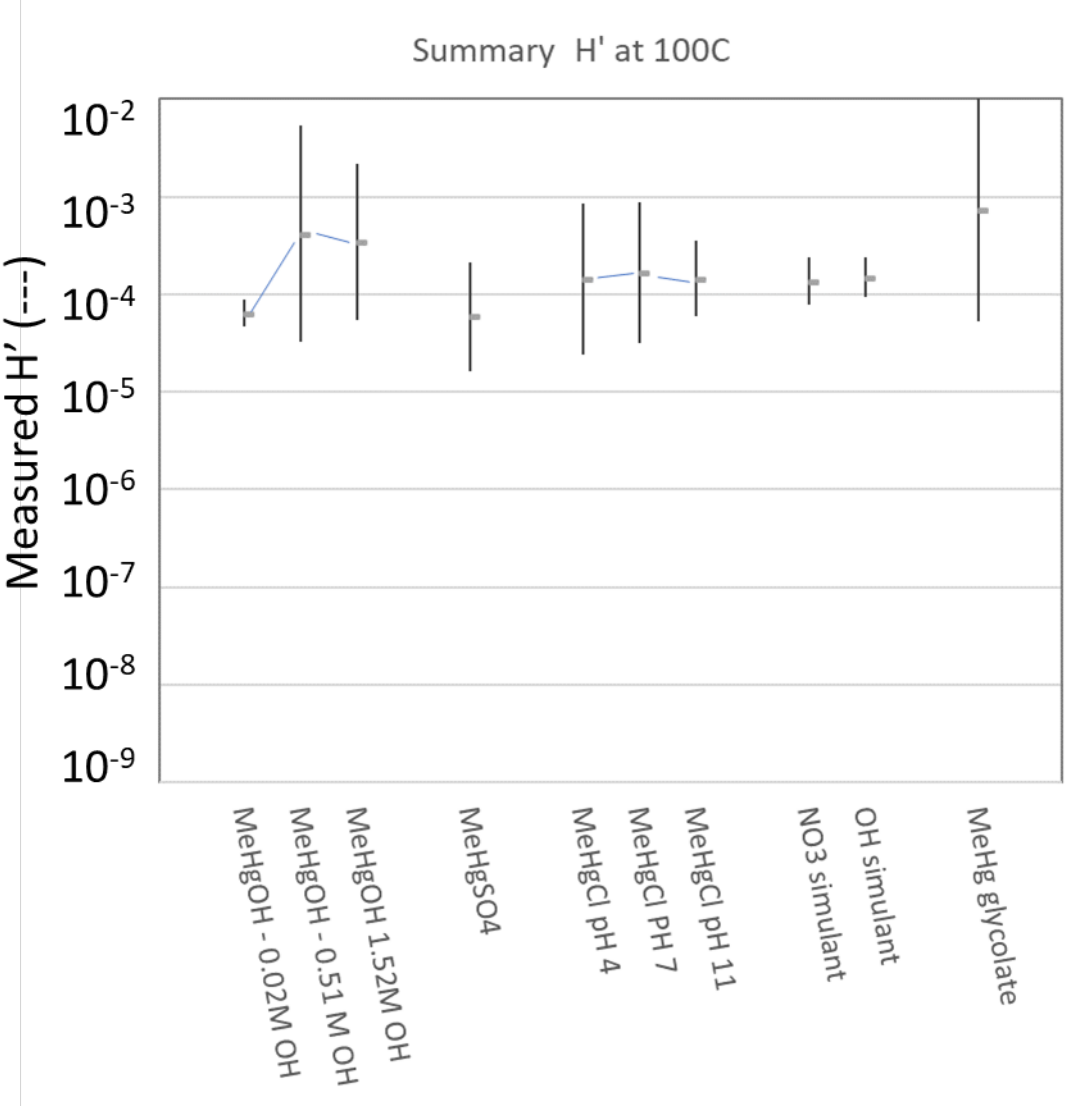

Figure 4-18. Summary H' at 100 °C

4.2 Vapor Pressure Determination and Solubility Evaluation

For those methylmercury compounds that precipitated in the microcosms, we also collected data on vapor pressure and solubility. The compounds that were amenable to this strategy were CH_3HgCl, CH_3HgSO_4, and CH_3Hg glycolate. No CH_3Hg^+ precipitated in any of the CH_3HgOH microcosms. Similarly, no CH_3Hg^+ precipitated in the two LWS simulants. This is consistent with the expected speciation in the high ionic strength and high hydroxide containing solutions typical of the LWS. The data on vapor pressure and solubility are presented in sequence below.

Vapor Pressure

The vapor pressure data and temperature projections for each compound are presented in a composite figure. The raw data and projections of vapor pressure as a function of temperature are depicted in the first graph assuming the linear August Equation for the projection (Equation 4-1). The August Equation is a simplified Antoine relationship (second graph):

Log10(vapor pressure) = A + B (1 / temperature in °C) ……..……...**Equation 4-1**

The simplified Antoine plots show the raw data as points and a projection line.

The figure numbering and order of the composite temperature dependent vapor pressure data plots and tables is as follows:

Figure 4-19 – Vapor pressure of CH_3HgCl
Figure 4-20 – Vapor pressure of CH_3HgSO_4
Figure 4-21 – Vapor pressure of CH_3Hg glycolate

Figure 4-19 exemplifies the data workup using the traditional format for the Antoine plots. In each case, vapor pressure is plotted on the y axis (using a log scale in gas phase concentration units of µg/L as Hg) as a function of temperature on the x axis (in units of °C). The coefficients (A and B) for the August equation are estimated based on the second graph that is formatted with the $\log_{10}$(vapor pressure) on the y axis and inverse temperature ($°C^{-1}$) on the x axis. The data are matched to the August equation by best fit of a linear regression. In the case of CH_3HgCl, the measured and predicted vapor pressure at 22 °C from this study can be compared to the literature values for this compound, in the range of 20 °C to 25 °C, as an initial validation step. As shown in Figure 4-19, there is a good agreement of the results from this study with the literature values, providing initial validation for the assumption of vapor pressure in the gas phase in the presence of precipitated solid material in the microcosm. This result also supports the straightforward headspace paradigm developed by SRNL as well as the analytical protocols (reagent preparation, gas and liquid subsampling, mercury trapping for gas samples, filtering and serial dilutions for liquid samples, and mercury quantification using the Milestone DMA-80).

The vapor pressure for CH_3HgCl and CH_3HgSO_4 were similar in magnitude. The estimated vapor pressure for glycolate based on total mercury assuming no conversion to a more volatile species was slightly higher than the other compounds.

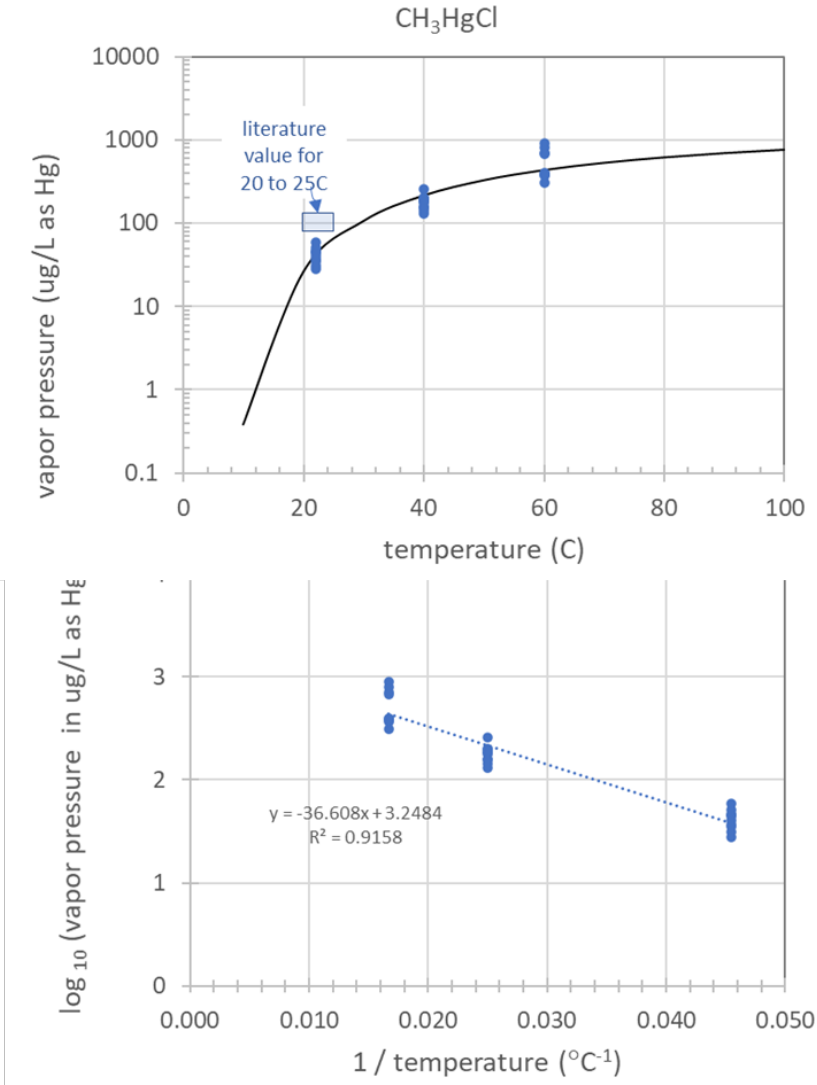

CH_3HgCl

	Vapor Pressure	
temperature C	µg/L as Hg	ρ (mm Hg)
10	0.4	0.00004
20	26	0.0024
30	107	0.0099
40	215	0.020
50	328	0.030
60	435	0.040
70	531	0.049
80	618	0.057
90	694	0.064
100	763	0.071

Figure 4-19. Projected CH_3HgCl Vapor Pressure (mg/L as Hg) as a Function of Temperature

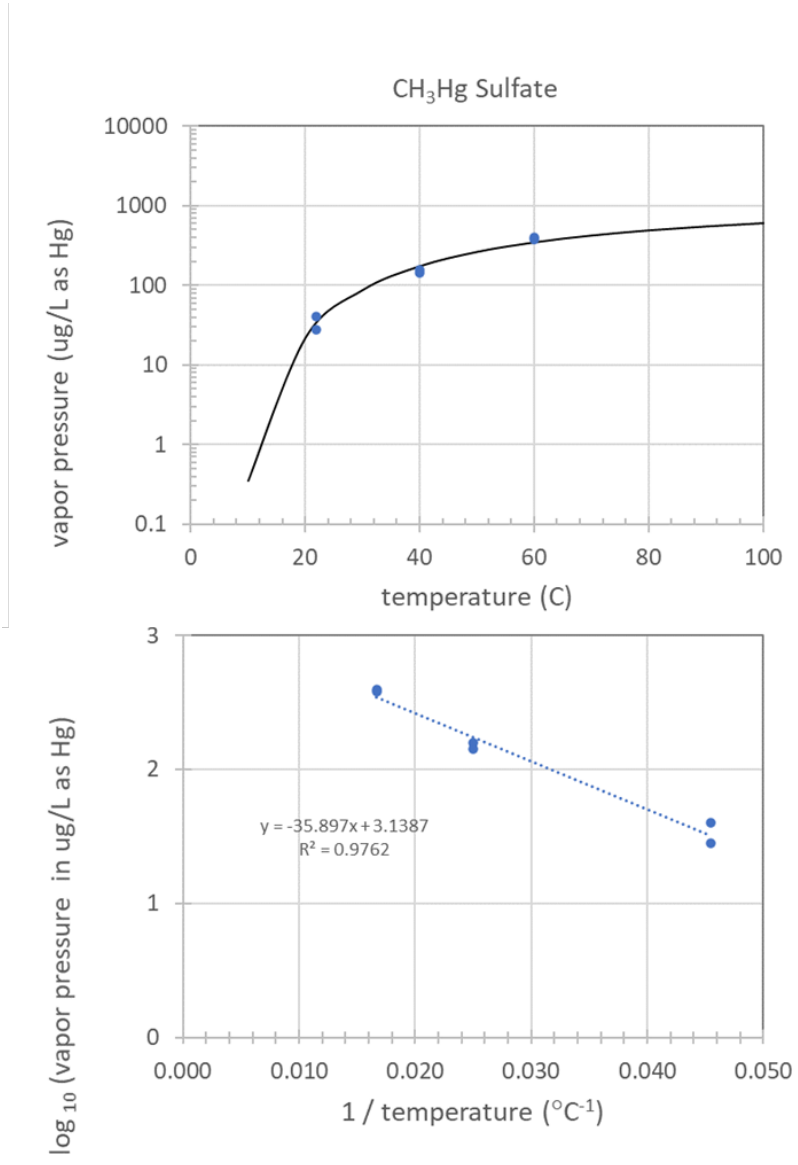

CH_3Hg Sulfate

	Vapor Pressure	
temperature C	µg/L as Hg	ρ (mm Hg)
10	0.35	0.00003
20	22	0.0020
30	88	0.0081
40	174	0.016
50	263	0.024
60	347	0.032
70	423	0.039
80	490	0.045
90	549	0.051
100	602	0.056

Figure 4-20. Projected CH_3HgSO_4 Vapor Pressure (mg/L as Hg) as a Function of Temperature

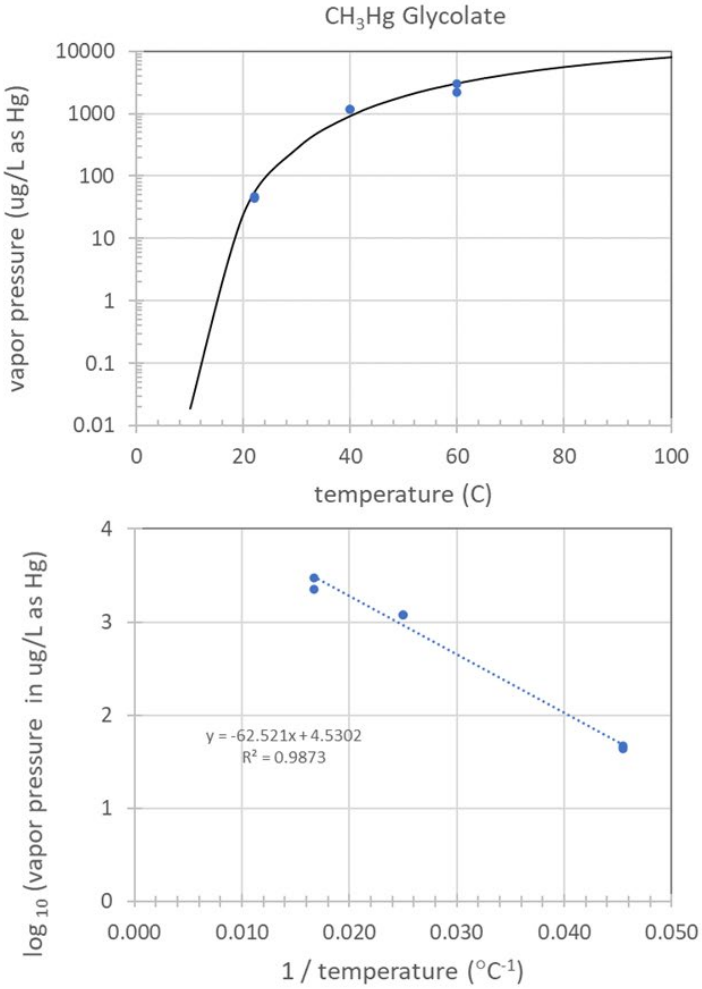

CH_3Hg Glycolate

	Vapor Pressure	
temperature C	µg/L as Hg	ρ (mm Hg)
10	0.019	0.000002
20	25	0.0024
30	279	0.026
40	927	0.086
50	1904	0.18
60	3077	0.29
70	4336	0.40
80	5606	0.52
90	6847	0.63
100	8035	0.75

Figure 4-21. Projected CH_3Hg Glycolate Vapor Pressure (mg/L as Hg) as a Function of Temperature

Solubility

The solubility data and temperature projections for each compound are presented in a composite figure. The projections of solubility as a function of temperature assume a simple enthalpy of solution relationship. The composite figures are comprised of two graphs and a table of data. The first graph for each compound shows the raw data (points) and the best estimate projection line. The second graph is used to estimate the enthalpy of solution by best fit. Note that in this section of the report, the liquid concentrations are reported in mg/L as Hg to be more consistent with the predominant units used in the scientific literature – the raw dataset and the liquid concentration values used in calculating H' were in units of ng/mL (i.e., µg/L) as Hg.

The figure numbers and order of the associated temperature dependent solubility data plots and tables are as follows:

Figure 4-22 – Solubility of CH_3HgCl
Figure 4-23 – Solubility of CH_3HgSO_4
Figure 4-24 – Solubility of CH_3 Hg glycolate

Figure 4-22 exemplifies the data workup using the traditional format for the enthalpy of solution data analysis. In each case, solubility is plotted on the y axis (in solution concentration units of mg/L as Hg) as a function of temperature on the x axis (in units of °C or °K). The enthalpy of solution is estimated using a second plot in which the y axis is $\ln(C_{295}/C_T)$ and the x axis is (295 - T)/(295 x T); where T is the absolute temperature of interest in °K, C_{295} is the solution concentration at 295 °K (22 °C), and C_T is the concentration at temperature T. The enthalpy of solution is calculated by multiplying the slope of the graph by the universal gas constant (R) in appropriate units. In the case of CH_3HgCl, the measured and predicted solubility at 22 °C from this study can be compared to the literature values for this compound in the range of 20 °C to 25 °C as an initial validation step. As shown in Figure 4-22, there is good agreement of the results from this study with literature values that provides initial validation of the assumption of solubility in the liquid phase in the presence of precipitated solid material in the microcosm. This result also supports the straightforward headspace paradigm developed by SRNL, as well as the analytical protocols (reagent preparation, gas and liquid subsampling, mercury trapping for gas samples, filtering and serial dilutions for liquid samples, and mercury quantification using the Milestone DMA-80).

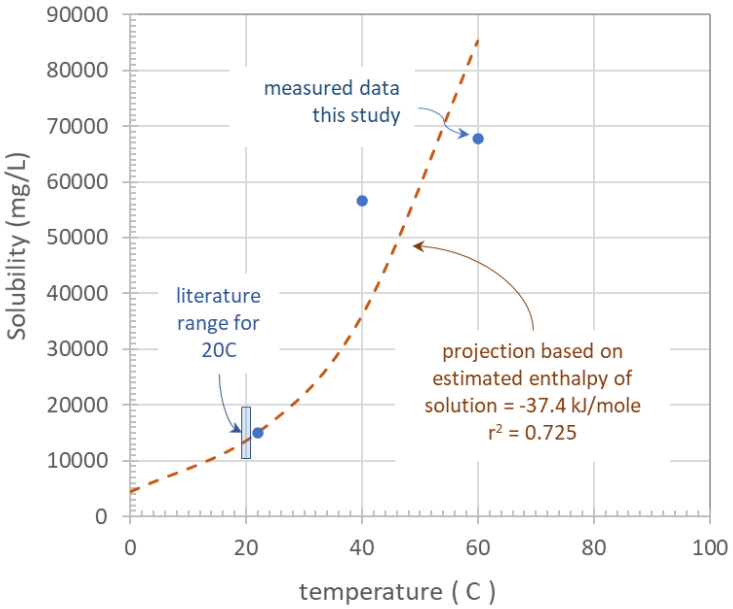

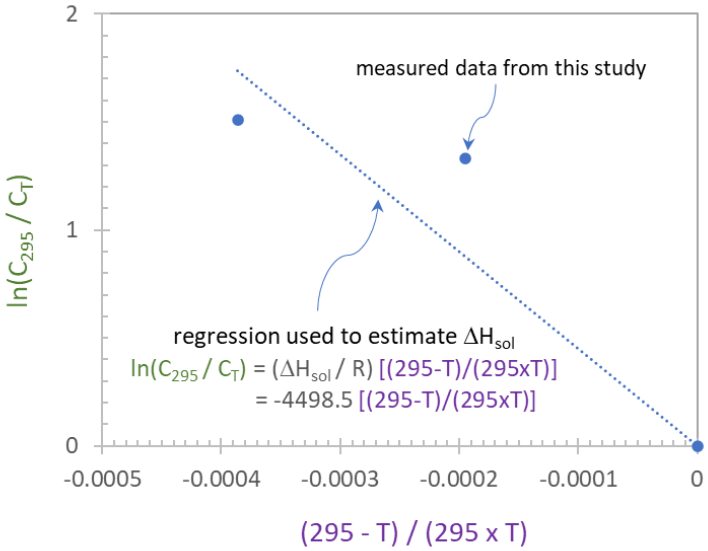

CH_3HgCl

temperature		model
(C)	(K)	**prediction**
0	273.3	4871
20	293.3	15000
40	313.3	40008
60	333.3	94849
80	353.3	203907
100	373.3	403821

Figure 4-22. Projected CH_3HgCl Solubility (mg/L as Hg) as a Function of Temperature (°C)

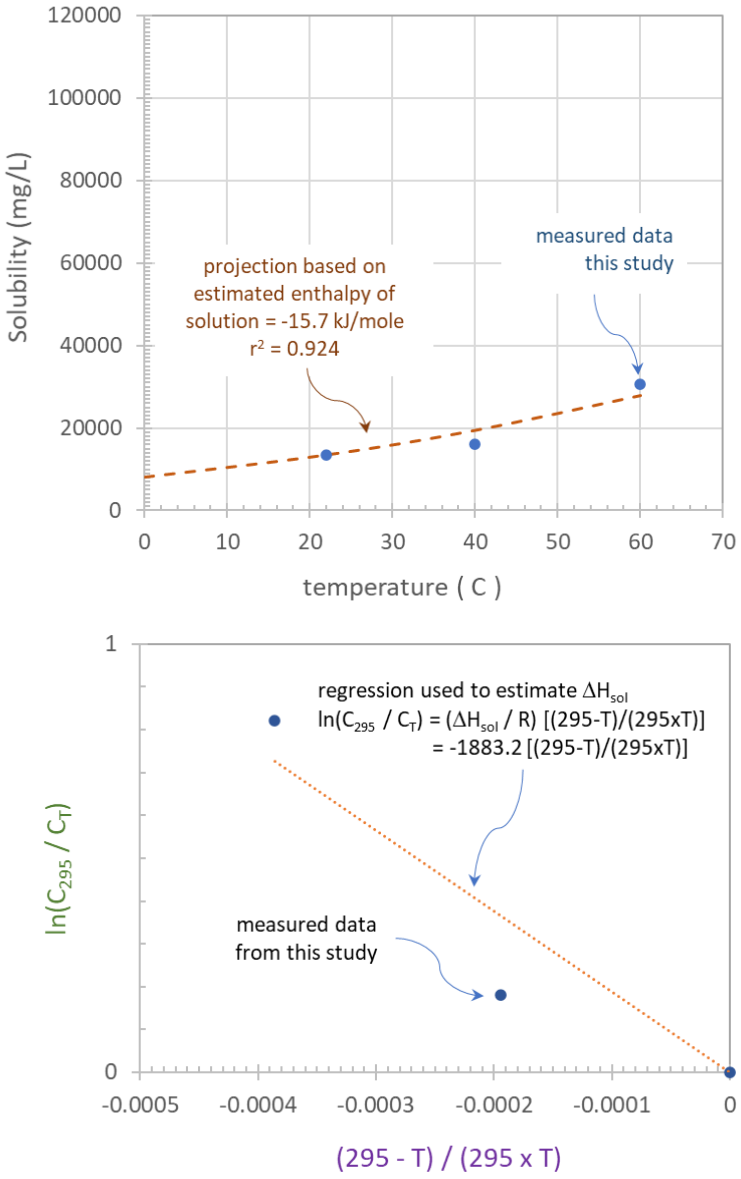

CH₃Hg Sulfate		
temperature		**model**
(C)	(K)	**prediction**
0	273.3	4377
20	293.3	13480
40	313.3	35954
60	333.3	85237
80	353.3	183245
100	373.3	362900

Figure 4-23. Projected CH_3HgSO_4 Solubility (mg/L as Hg) as a Function of Temperature (°C)

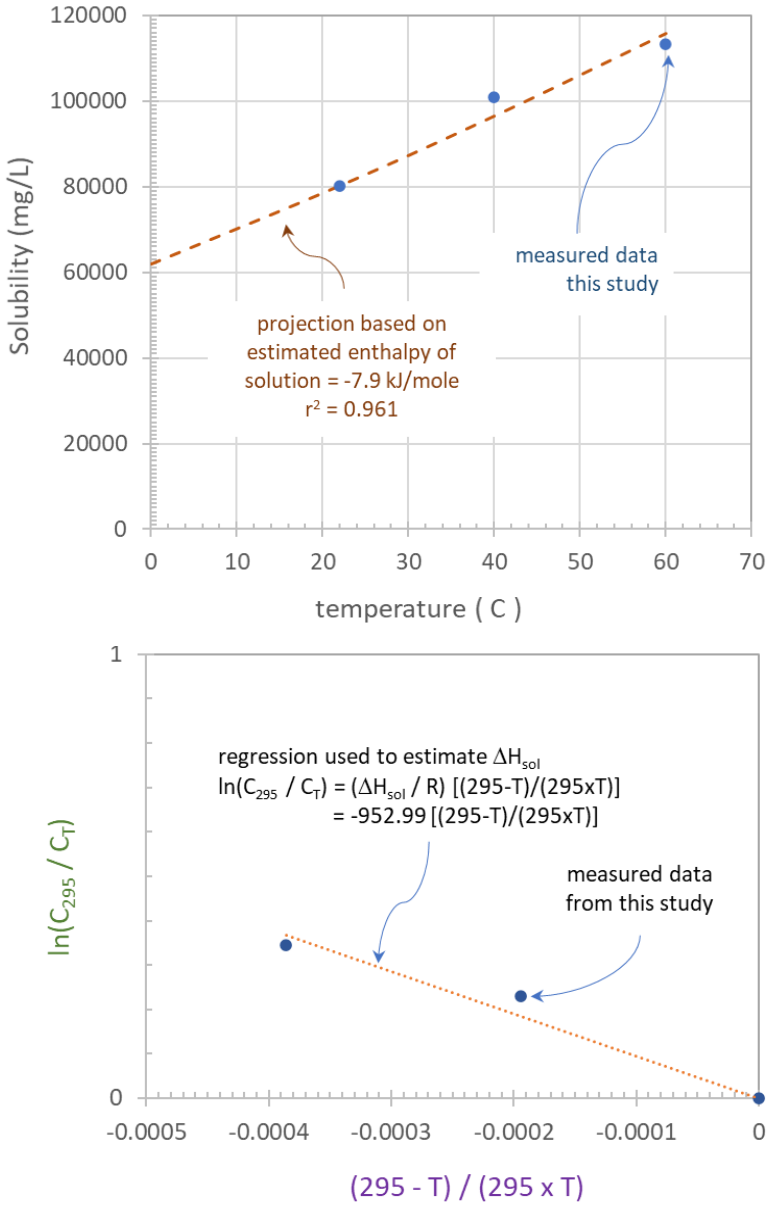

CH_3Hg Glycolate		
temperature		**model**
(C)	(K)	**prediction**
0	273.3	26041
20	293.3	80195
40	313.3	213898
60	333.3	507093
80	353.3	1090157
100	373.3	2158960

Figure 4-24. Projected CH_3Hg Glycolate Solubility (mg/L as Hg) as a Function of Temperature (°C)

The measured solubility of the various methylmercury compounds for three example temperatures is tabulated below (Table 4-1).

Table 4-1. Summary of the Measured Raw Data for Solubility of Representative Methylmercury Compounds.

X =	Average measured solubility (mg/L as Hg)			$\Delta H_{solubility}$ (kJ/mole)
	22 °C	40 °C	60 °C	
OH [1]	> 200,000	> 200,000	> 200,000	n/a
Cl	15,000	56,700	67,750	-37.4
SO_4	13,480	16,151	30,625	-15.7
Glycolate [2]	80,195	101,000	113,250	-7.9
Formate [3]	n/a	n/a	n/a	n/a

[1] CH_3HgOH was soluble under all experimental conditions.
[2] CH_3Hg glycolate solubilities may be higher at elevated temperatures because the measured solubilities accounted for most or all of the added mass in the microcosms.
[3] CH_3Hg formate solubility was not estimated because the starting materials were lost, reacting to form dimethylmercury.

4.3 Observed Dimethylmercury Synthesis in Aqueous Solution

The microcosm containing 0.5 M methylmercury and 0.5 M formate resulted in rapid accumulation of mercury in the vapor phase and headspace concentrations of total mercury that were significantly higher than expected at 22 °C. During the initial gas subsampling of this system, the microcolumn trap collected approximately 1000 x the expected mass of mercury (>>1000 ng), which is well above the operational range of the Milestone DMA-80. Analysis of the microcolumn resulted in overloading and damaging the Milestone DMA analyzer and necessitating a complete cleaning and replacement of all internal consumable components, including the catalyst and amalgamator.

After the rebuild, microcosm headspace gas was collected and diluted in clean air (DF 10). Two microliters of the diluted gas were applied to an the adsoquick trap to collect the mercury for analysis. The resulting samples confirmed that the headspace in the formate microcosms contained high levels of mercury-containing compounds. The results for duplicate microcosms were 1,625,000 ng/mL and 1,684,000 ng/mL of mercury, which equates to gases containing mercury comprising 16% and 16.6 % by volume in the microcosm headspace. These concentrations are considered estimates since the amount of mercury on the traps was still higher than the 300 ng upper calibration standard. Importantly, the measured headspace concentrations were several orders of magnitude above expected values bases on Henry's Law partitioning between a solution and a gas phase and significantly above the vapor pressure of elemental Hg^0.

The results indicate a chemical reaction occurs between formate and methylmercury, resulting in the generation of a more volatile mercury compound. With the addition of a second covalently bound methyl group, dimethylmercury is comparably a more volatile mercury species with a documented vapor pressure (approximately 8% by volume) that is similar to the estimated/measured values in the headspace. In designing the experiments, abiotic formation of $(CH_3)_2Hg$ in aqueous solution was considered unlikely since it has not been documented in the literature to occur in any significant extent with these or similar reagents. However, the research team called a time-out and developed a plan to further assess the unexpected result. The research team isolated the microcosms and initiated steps to identify the reason(s) for the high headspace mercury levels.

Several follow-up actions were taken to determine the nature/form of the mercury in the headspace gas, including: a) a scoping nuclear magnetic resonance (NMR) measurement that suggested a rapid and relatively complete conversion of CH_3Hg^+ to covalently bonded synthesis products and b) a subsequent gas chromatography- mass spectroscopy (GC-MS) study that provided definitive identification of $(CH_3)_2Hg$ as a principal end product of the synthesis reaction(s). The scoping study using NMR was performed by mixing a trace quantity of 1 M CH_3HgOH and 1 M formic acid in an NMR tube and then scanning changes in mercury and carbon bonding in the liquid phase at various times. Scoping results confirmed formation of covalent C-Hg bonds at early times. The scoping NMR also indicated that the synthesis reaction was rapid and relatively complete since the signal in solution dissipated within about five minutes in a purged NMR tube as the products partitioned out of solution into the vapor phase and were vented into the chemical hood. The follow-on GC-MS study provided definitive identification of $(CH_3)_2Hg$ and confirmed the existence of a high-yield aqueous synthesis reaction. The GC-MS study is described in more detail below.

1) Samples from the formate microcosms were prepared for analysis on the purge and trap as follows:
   a) Arrangements were made for transporting the prepared gas samples to the limited area from 999-1W prior to preparing the samples to assure that the analysis as soon as possible after collection.
   b) A clean-standard 40 mL screw top septum vial was loaded with 15 mL of Hg-free DI water and capped. One milliliter of gas was withdrawn from the vial using a gas tight syringe to generate slightly underpressurized condition to minimize the potential for loss of analyte during transport and storage.
   c) A measured volume of headspace gas was added to the vial. Vials were prepared at two different spike levels: 3 µL and 30 µL of headspace gas. These spike quantities were selected to provide the appropriate signal on the GC-MS based on past analysis of $(CH_3)_2Hg$ in samples from the SRS LWS.
   d) The use of a standard vial facilitates straightforward introduction of microcosm headspace gas into the existing GC-MS system.
   e) Samples were transported to 773-A for analysis using purge and trap GC-MS.
2) Upon receipt of the sample, the sealed glass vial was kept cold at approximately 4 ˚C.
3) The glass vial is placed into the autosampler tray of the purge and trap GC-MS.
4) The sample is purged with helium for 11 minutes at a flow rate of 40 mL/minute.
5) During purge, 20 µL of a deuterated volatile organic internal standard mixture (2000 mg/L) is automatically added by the instrument.
6) The purged gas is passed through a 24 cm column containing Tenax at 20 °C to trap organic and organomercury compounds.
7) Following the purge, the Tenax trap is desorbed for 2 minutes at 180 °C and any desorbed compounds are passed via heated transfer line to the GC-MS.
8) The GC is operated in split injection mode at a ratio of 1:100.
9) The organic compounds are separated on a DB-5 GC column (30 m x 0.25 mm ID x 1 µm film thickness).
10) The GC oven is programmed to hold at 35 °C for 1 minute and increase at a rate of 20 °C/minute to a final temperature of 180 °C, where it will hold for 5 minutes.
11) The mass spectrometer is operated in scanning mode over a range of 30 m/z to 450 m/z.

Two samples were analyzed by purge and trap GC-MS: “30 DMM” (containing 30 µL of headspace gas) and “3 DMM” (containing 3 µL of headspace gas). $(CH_3)_2Hg$ was detected in both samples. Figure 4-25 shows the full chromatogram associated with “30_DMM”, showing the six spiked internal standards. $(CH_3)_2Hg$ can be seen as a small shoulder peak preceding the internal standard peak at 2.9 minutes. Figure 4-26 shows the chromatogram when selecting only for the 217 m/z ion. That ion is the highest intensity mercury fragment in the NIST library mass spectrum for $(CH_3)_2Hg$, which corresponds to the mass following ionization and loss of one methyl group. Figure 4-27 demonstrates the NIST library match of

dimethylmercury to the reaction product of formate and methylmercury. Figure 4-28 and Figure 4-29 show the full chromatogram and isolated ion chromatogram at 217 m/z for the sample labeled "3_DMM".

When comparing with the closest internal standard peak (1,3-diflurobenzene), assuming the same relationships between signal and mass, the $(CH_3)_2Hg$ was quantified at 1.38 µg in the sample labeled "30_DMM" and 0.266 µg in "3_DMM." This equates to headspace concentrations of 46,000 ng/mL and 88,700 ng/mL, which are about 30 times lower than measurement results using direct mercury analysis. Given the uncertainties in estimation, the sample handling/transport and storage of the GC-MS samples, and the likelihood that the GC-MS signal response for $(CH_3)_2Hg$ may differ from 1,3-diflurobenzene, these results are considered to be reasonably similar for purposes of the scoping evaluation.

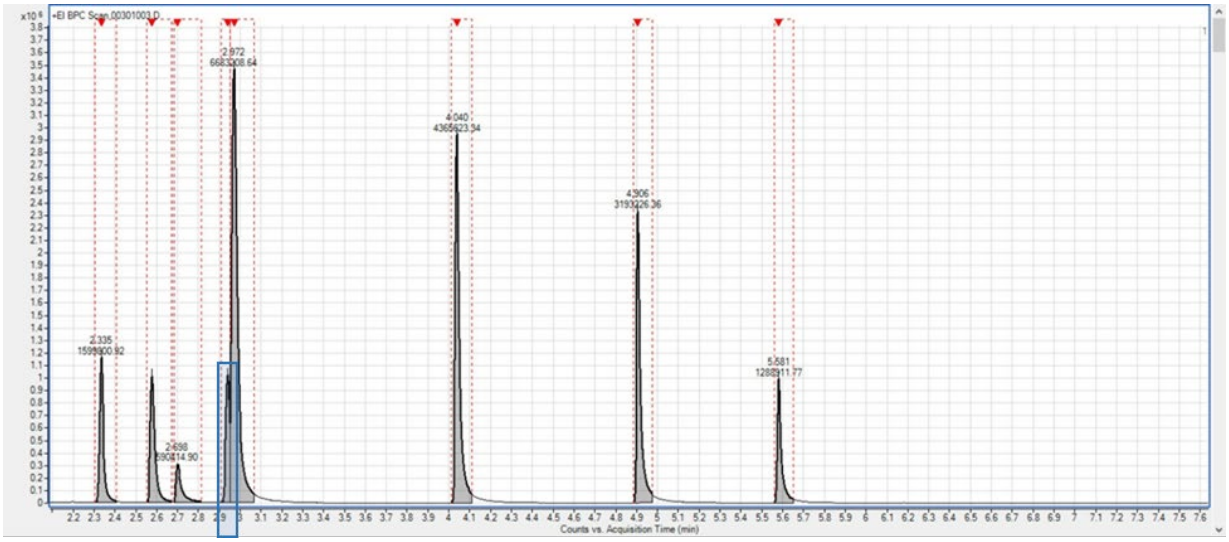

Figure 4-25. Full Chromatogram of "30_DMM" Showing Dimethylmercury Peak (Blue Box)

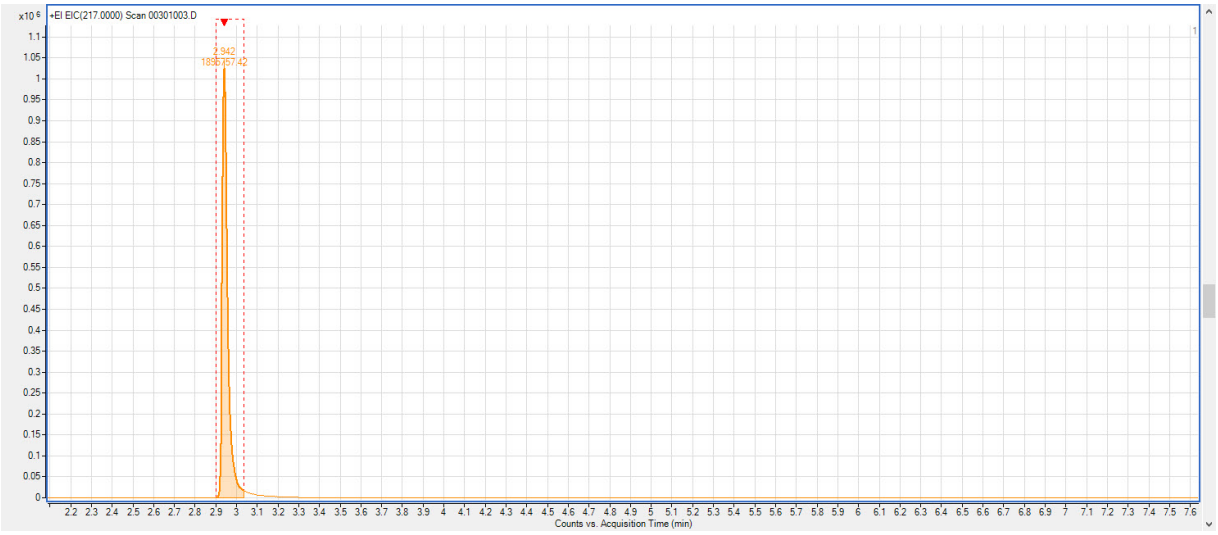

Figure 4-26. Chromatogram Selecting for 217 m/z Ion in "30_DMM"

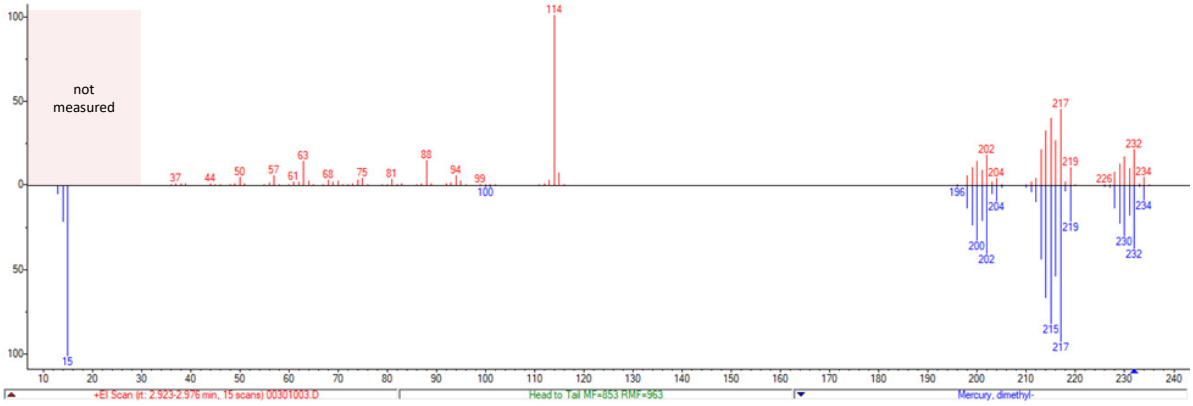

Figure 4-27. Match of NIST Library Mass Spectrum for $(CH_3)_2Hg$ to the Unknown Compound from Figure 4-26[a]

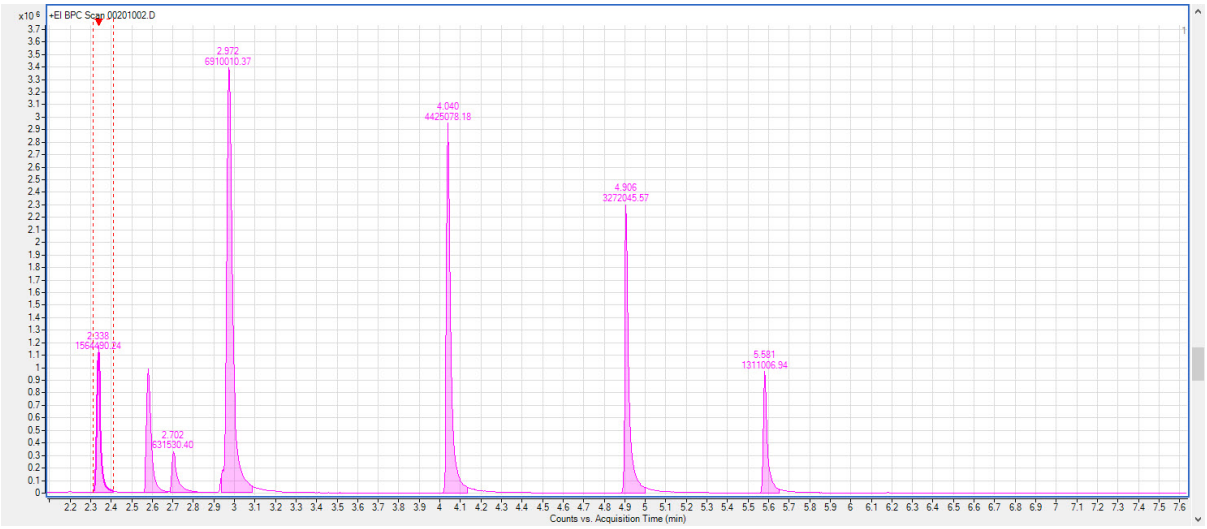

Figure 4-28. Full Chromatogram of "3_DMM"

[a] Red lines are data acquired by SRNL (including the co-eluting internal standard peak at 114 m/z) and blue lines are the library reference for dimethylmercury

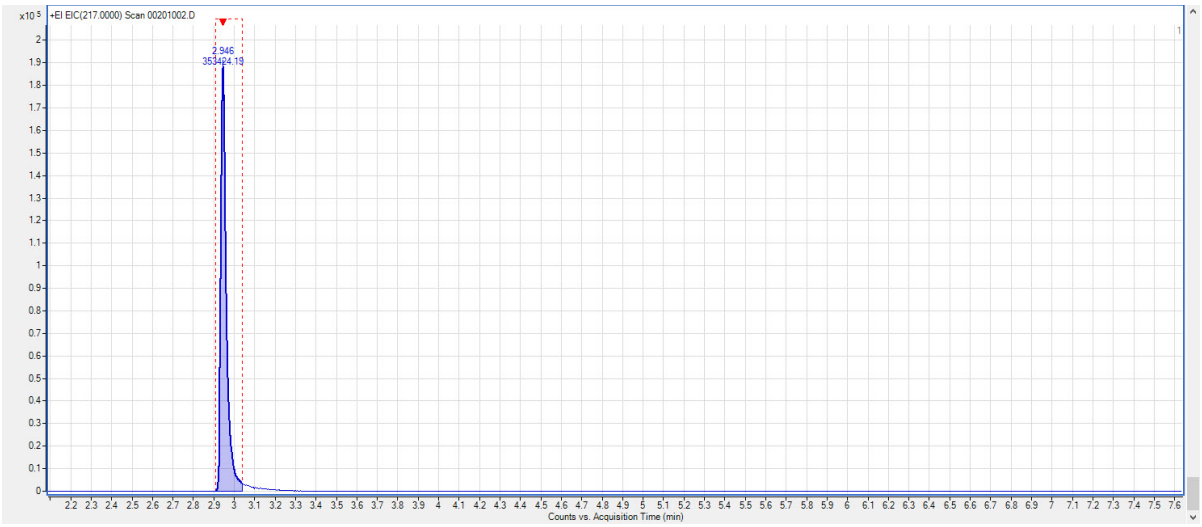

Figure 4-29. Chromatogram Selecting for 217 m/z Ion in "3_DMM"

GC-MS confirmed synthesis of $(CH_3)_2Hg$ in a solution of 0.5 M CH_3HgOH and 0.5 M formic acid (i.e., CH_3Hg^+ and formate). Based on this finding, the research team evaluated the scientific literature using a wider lens to develop a conjectural reaction mechanism. The most likely mechanisms involved formation of an intermediate methylmercury hydride. This hydride formation is documented in Filippelli et al. (1992). In their research, a labile methylmercury hydride moiety was formed in aqueous solution using sodium borohydride reagent as a derivatization step in an analytical protocol. They determined that the methylmercury hydride was "a volatile and unexpectedly stable species which had a half-life of approximately 2 h {in dilute aqueous solution}". The generated methylmercury hydride was analyzed using GC and they concluded that their results suggest a "need to investigate further the occurrence in nature of this highly volatile and unexpectedly stable species". Formate has also been used as a reagent for generating hydrides, suggesting the possibility of the following conjectural reaction mechanism consisting of two steps: 1) reaction of formate with CH_3Hg^+ to from a relatively volatile and labile methylmercury hydride, and 2) a disproportionation reaction involving two methylmercury hydride molecules to form $(CH_3)_2Hg$ and Hg^0. Based on Filippelli et al. (1992), these reactions would be expected to occur over a finite timeframe (hours) and would eventually result in the conversion of the starting CH_3Hg^+ to the disproportionation products. The observations in the formate microcosms suggests reaction rates that are significantly faster (minutes), perhaps due to the high starting concentrations of reagents or differences in kinetics considering the initiation of the process by formate versus sodium borohydride. The reaction mechanism can be visualized as follows (Figure 4-30).

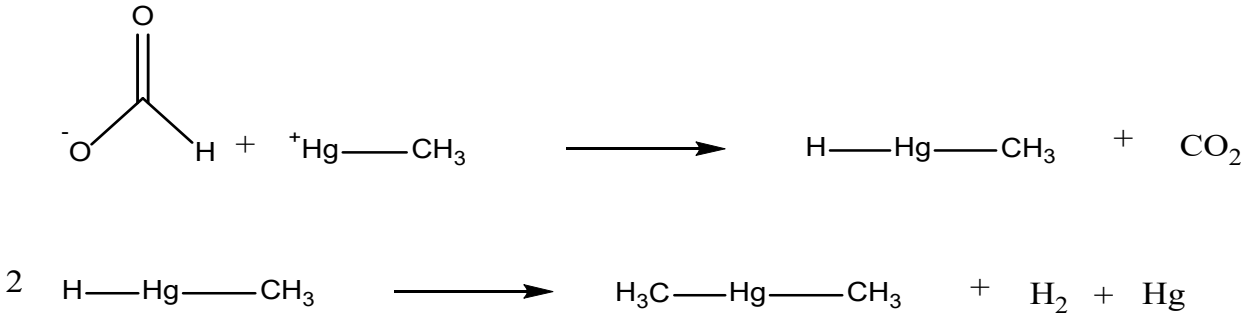

Figure 4-30. Conjectural Reaction Mechanism for Dimethyl Mercury Synthesis

The literature documents that formic acid is commonly used in reductive amination (Wallach reaction) as an alternative to $NaBH_4$. For example, Aguilo (1969) documents formic acid as a potential hydride source when used with Pd, and by extension mercury. Khriachtchev et al. (2002) used lasers to facilitate formic acid reacting to form hydrogen and carbon dioxide, a reaction that required cis form; thus, documenting that conformation may be a factor. Finally, Torchy and Barbry (2001) documented a modified Eschweiler-Clarke reaction using formic acid as a hydride source. Eschweiler Clarke is a principal reaction that demonstrates that formic acid used as a hydride source where the electrophile is an enamine (Figure 4-31).

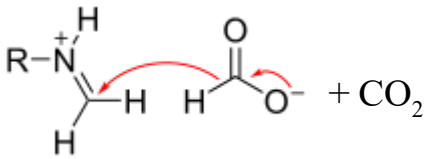

Figure 4-31. Eschweiler Clarke Reaction

In the enamine system, several related reaction mechanisms from the literature link to the key hydride step. Notable steps include the Leuckart Reaction in which ammonium formate acts as a reductant to form the enamine from an aldehyde or ketone and the Cannizzaro Reaction in which an analogous disproportionation step is demonstrated. During the Cannizzaro Reaction, a redox reaction involving transfer of a hydride from one substrate molecule to another occurs where one aldehyde is oxidized to form the acid and the other is reduced to form the alcohol. In our case, the putative electrophile is CH_3Hg^+ instead of the enamine, and the subsequent disproportionation resulted in the production of $(CH_3)_2Hg$ and Hg^0. Supporting the conjectural reaction thermodynamically are the following driving forces whose signs (+/-) were calculated from the proposed products and reactants: $\Delta S = (+)$, $\Delta H = (-)$, $\Delta G = (-)$.

Note that other reaction pathways may be governing the observed transformations. Additional study is needed to understand and document both the mechanism and kinetics. For example, demonstrating the formation of both $(CH_3)_2Hg$ and Hg^0 in the correct ratio would support the general concepts of synthesis and disproportionation and confirmation of reaction kinetics by examining both C and Hg using NMR.

The data confirmed that the microcosms with formate resulted in chemical conversion of the reactants into dimethylmercury with very high (volume % level) concentrations of mercury in the headspace. This behavior can be contrasted with the glycolate microcosms. As described above, the headspace concentrations in the glycolate microcosm were slightly elevated compare to the chloride and sulfate microcosms. While higher measured concentration in the headspace gas in the glycolate microcosm could be influenced by the formation of a trace amount of dimethylmercury or a similar product, the amount of mercury in the headspace of the glycolate microcosms was about 1000x lower than the formate microcosms. Based on these data, the amount of dimethylmercury formed with glycolate (if any) was much significantly less.

At this juncture, we have observed the formation of $(CH_3)_2Hg$ in the formate microcosms and confirmed the likelihood of a high-yield aqueous synthesis reaction. While we were working in high concentrations (e.g., 0.5 M CH_3Hg^+ and 0.5M formate) that are not representative of the LWS, the results may have implications that are relevant to the LWS; including field observation of trace $(CH_3)_2Hg$ in tank headspaces, for example. These results could also inform LWS scientists and engineers working on flowsheet development.

5.0 Conclusions

The studies confirmed that there are low but measurable concentrations of methylmercury in the headspace gas in contact with high concentration solutions. Methylmercury partitioning (H') was measured as a function of temperature and the findings suggest an increase of three to four orders of magnitude in partitioning into the vapor phase as temperatures increase from ambient (20 ˚C) to the boiling point of aqueous solutions (near/above 100 ˚C). These experiments generated data that can be used to better assess partitioning as a function of temperature: a) for methylmercury hydroxide in simulants and in solutions of varying ionic strength, b) for methylmercury sulfate, c) for methylmercury chloride in solutions of varying pH, and d) for methylmercury glycolate. For those compounds that precipitated in the microcosms (methylmercury chloride, methylmercury sulfate, and methylmercury glycolate), vapor pressure and solubility were also determined.

The data were collected using a streamlined static headspace analysis strategy in replicate microcosms. Gas and liquid subsamples were quantified using SRNL-developed, optimized methods that rely on direct mercury analysis as the final quantification step. Over 200 individual sample results were generated during the study.

At 20 ˚C, the partitioning, vapor pressure, and solubility measurements in this study closely matched the available scientific literature, providing initial validation of the static headspace strategy and the analysis protocols. In dilute solutions, the H' for methylmercury hydroxide was about four orders of magnitude lower than the H' for methylmercury chloride. These compounds bracket the expected range of H' for methylmercury compounds partitioning from aqueous solution into a gas phase.

The H' for methylmercury hydroxide increased significantly as a function of ionic strength, documenting a salting out effect. The H' value in the high ionic strength microcosms increased by about two orders of magnitude. In the high ionic strength trial, the measured H' closely matched the values measured in the LWS simulant solutions.

The measured H' increased as a function of increasing temperature and the relationship was reasonably described using the Van't Hoff Equation. The measured vapor pressures increased as a function of temperature and the relationship can be reasonably described using the August Equation, which is a simplified form of the Antoine Equation. The measured solubilities increased as a function of temperature and the relationship can be reasonably described using an estimated enthalpy of solution.

At low temperatures and high ionic strength, the H' measurements for all compounds except CH_3HgCl were in a similar range. Since chloride is procedurally limited in the LWS system, this finding provides the opportunity to develop scoping H' values for SRR scientists and engineers to use in developing flowsheets and managing LWS operations. Further, as temperature increased, the estimates for H' trended to a similar and consistent value/magnitude for all compounds, including CH_3HgCl, and all ionic strengths and measured pHs. This inherent robustness in the emergent data is significant because it supports parameter estimates for the potential range of LWS conditions that are insensitive to specific solution conditions. The following table (Table 5-1) provides scoping ranges for H' over a range of temperatures:

Table 5-1. Scoping Ranges for Dimensionless Henry's Law Coefficient as a Function of Temperature.

Temperature (°C)	Estimate of H'
20	5×10^{-7}
40	3×10^{-6}
60	2×10^{-5}
80	1×10^{-4}
100	3×10^{-4}
>100 (evaporator)	1×10^{-3}

This research was primarily intended to provide parameters for SRR scientists and engineers to make flowsheet and design calculations. However, an additional, potentially significant finding was identified while performing the experiments. In microcosms where methylmercury was added in the presence of formate, significant quantities of dimethylmercury were synthesized in the aqueous solution and partitioned into the headspace. The fugacity of the mercury species in the formate microcosms was higher than expected; orders of magnitude higher than that of methylmercury glycolate methylmercury chloride, and methylmercury hydroxide. The unexpected finding was validated by independent analysis and a reaction mechanism was developed. The report documents this finding to help inform flowsheet decision and provide insight into this mechanism as a potential contributor to the observations that trace levels of dimethylmercury are being measured by SRR industrial hygienists in the headspace of some of the key waste tanks.

6.0 Recommendations, Path Forward, or Future Work

This work extends the efforts of Meraw (2015) who appropriately concluded that methylmercury does not significantly contribute to LWS flammability safety risks. This additional information may be useful in evaluating other types of methylmercury behaviors in the LWS. Although this work examined a range of common anions/compounds it is not exhaustive. However, the information provides a sound technical basis for general consideration of the partitioning of methylmercury between LWS solutions and headspace gases. Methylmercury is expected to comprise only a small fraction of the headspace mercury. Concentrations are expected to be lower than that of Hg^0 or dimethyl mercury (if present). Nonetheless, understanding the physical and chemical properties of this dominant mercury moiety within the LWS is important in disciplined operations. Future work to elucidate the identified dimethylmercury abiotic aqueous synthesis pathway is recommended.

7.0 References

Aguilo, A. (1969) Palldium (II) – Catalyzed Oxidation of Formic Acid in Acetic Acid Solution. *J. Catal.* 13, 283-289.

Alderighi, L., Gans, P., Midollini, S., Vacca, A. (2003) Co-ordination Chemistry of the Methylmercury(II) Ion in Aqueous Solution: a Thermodynamic Investigation. *Inorganica Chimica Acta* 356: 8 -18.

Bloom, N.S, Von der Geest, E., Presto, E.M., Wilmarth, W., Thaxton, D. (2004) Formation and Degradation of $(CH3)_2Hg$ in Nuclear Waste Tanks.

EPA (2007) Mercury in Solids and Solutions by Thermal Decomposition, Amalgamation, and Atomic Absorption Spectrophotometry. Method 7473. Revision 0.

EPA, 2017. EPI Suite™-Estimation Program Interface. U.S. Environmental Protection Agency Office of Pollution Prevention and Toxic Risk Assessment Division. https://www.epa.gov/tsca-screening-tools/epi-suitetm-estimation-program-interface.

EPA (2021) EPA On-line Tools for Site Assessment Calculation – Henry's Law Conversions. https://www3.epa.gov/ceampubl/learn2model/part-two/onsite/henryslaw.html

Filippelli, M., Baldi, F., Brinckman, F.E., and Oison, G.J. (1992) Methylmercury Determination as Volatile Methylmercury Hydride by Purge and Trap Gas Chromatography in Line with Fourier Transform Infrared Spectroscopy, *Environmental Science and Technology*, 26:1457-1460.

Iverfeldt, A. and Lindqvist, O. (1982) Distribution Equilibrium of Methyl Mercury Chloride Between Water and Air. *Atmospheric Environment* 16:12, 2917-2925.

Iverfeldt, A. and Persson, L. (1985) The Solvation Thermodynamics of Methylmercury(II) Species Derived from Measurements of the Heat of Solution and the Henry's Law Constant. *Inorganic Chimica Acta*. 103, 113-119

Kanzler, C.R., Lian, P., Trainer, E.L., Yang, X., Govind, N. Parks, J.M., and Graham, A. M. (2017) Emerging Investigator Series: Methylmercury Speciation and Dimethylmercury Production in Sulfidic Solutions. *Environ. Sci.: Processes Impacts*. DOI: 10.1039/c7em00533d

Khriachtchev, L., Macoas, E., Pettersson, M., and Rasanen, M. (2002) Conformational memory in photodissociation of formic acid. *J. Am. Chem. Soc.* 124, 10994-10995.

Long, L.H. and Cattanach, J. (1961) Antoine Vapour-Pressure Equations and Heats of Vaporization for the Dimethyls of Zinc, Cadmium, and Mercury. *J. Inorg. Nucl. Chem.* 20, 340-342.

Loux, N. (2007) An Assessment of Thermodynamic Reaction Constants for Simulating Aqueous Environmental Monomethylmercury Speciation. *Chemical Speciation & Bioavailability* 19:4, 183-196. DOI: 10.3184/095422907X255947

Meraw, H.J. (2015) Volatilization and Flammability Characteristics of Elemental and Organic Mercury. Savannah River Remediation.

Meuleman, C., Laino, C.C., Lansens, P., and Baeyens, W. (1993) A Study of the Behavior of Methyl Mercury Compounds in Aqueous Solutions, and of Gas/Liquid Distribution Coefficients, Using Head Space Analysis. *Wat. Res.* 27:9, 1431-1446

Talmi, Y. and Mesmer, R.E. (1975) Studies of Vaporization and Halogen Decomposition of Methyl Mercury Compounds Using a GC with a Microwave Detector. *Water Research* 9, 547-552

Torchy, S. and Barbry, D. (2001) N-alkylation of amines under microwave irradiation: modified Eschweiler-Clarke reaction. *J. Chem. Res.* (S) 292-293.

Appendix A.

RAW DATA FOR HENRY'S LAW, VAPOR PRESUURE AND SOLUBILITY STUDY

compound	chemical formula	solution conditions	temperature (°C)	gas phase concentration (ng/mL as Hg)	liquid phase concentration (ng/mL as Hg)	notes
methyl mercury hydroxide	CH_3HgOH	DI Water (approx 0.02M OH^-)	20	0.93	1.00×10^8	1, 2
methyl mercury hydroxide	CH_3HgOH	DI Water (approx 0.02M OH^-)	20	0.82	1.00×10^8	1, 2
methyl mercury hydroxide	CH_3HgOH	DI Water (approx 0.02M OH^-)	20	0.64	1.00×10^8	1, 2
methyl mercury hydroxide	CH_3HgOH	DI Water (approx 0.02M OH^-)	20	0.92	1.00×10^8	1, 2
methyl mercury hydroxide	CH_3HgOH	DI Water (approx 0.02M OH^-)	40	10	1.00×10^8	1, 2
methyl mercury hydroxide	CH_3HgOH	DI Water (approx 0.02M OH^-)	40	12	1.00×10^8	1, 2
methyl mercury hydroxide	CH_3HgOH	DI Water (approx 0.02M OH^-)	40	15	1.00×10^8	1, 2
methyl mercury hydroxide	CH_3HgOH	DI Water (approx 0.02M OH^-)	70	318	1.00×10^8	1, 2
methyl mercury hydroxide	CH_3HgOH	DI Water (approx 0.02M OH^-)	70	387	1.00×10^8	1, 2
methyl mercury hydroxide	CH_3HgOH	DI Water (approx 0.02M OH^-)	70	376	1.00×10^8	1, 2
methyl mercury (various)	$CH_3Hg\{X\}$	NO_3 simulant	20	24	1.00×10^8	1, 2
methyl mercury (various)	$CH_3Hg\{X\}$	NO_3 simulant	20	34	1.00×10^8	1, 2
methyl mercury (various)	$CH_3Hg\{X\}$	NO_3 simulant	20	42	1.00×10^8	1, 2
methyl mercury (various)	$CH_3Hg\{X\}$	NO_3 simulant	40	303	1.00×10^8	1, 2
methyl mercury (various)	$CH_3Hg\{X\}$	NO_3 simulant	40	263	1.00×10^8	1, 2
methyl mercury (various)	$CH_3Hg\{X\}$	NO_3 simulant	40	282	1.00×10^8	1, 2
methyl mercury (various)	$CH_3Hg\{X\}$	NO_3 simulant	70	1566	1.00×10^8	1, 2
methyl mercury (various)	$CH_3Hg\{X\}$	NO_3 simulant	70	1950	1.00×10^8	1, 2
methyl mercury (various)	$CH_3Hg\{X\}$	NO_3 simulant	70	1985	1.00×10^8	1, 2
methyl mercury (various)	$CH_3Hg\{X\}$	OH simulant	20	47	1.00×10^8	1, 2
methyl mercury (various)	$CH_3Hg\{X\}$	OH simulant	20	53	1.00×10^8	1, 2
methyl mercury (various)	$CH_3Hg\{X\}$	OH simulant	20	48	1.00×10^8	1, 2
methyl mercury (various)	$CH_3Hg\{X\}$	OH simulant	40	414	1.00×10^8	1, 2
methyl mercury (various)	$CH_3Hg\{X\}$	OH simulant	40	427	1.00×10^8	1, 2
methyl mercury (various)	$CH_3Hg\{X\}$	OH simulant	40	310	1.00×10^8	1, 2
methyl mercury (various)	$CH_3Hg\{X\}$	OH simulant	70	2359	1.00×10^8	1, 2
methyl mercury (various)	$CH_3Hg\{X\}$	OH simulant	70	2165	1.00×10^8	1, 2
methyl mercury (various)	$CH_3Hg\{X\}$	OH simulant	70	2147	1.00×10^8	1, 2
methyl mercury chloride	CH_3HgCl	DI water pH approx 11	22	47	1.50×10^6	1, 3
methyl mercury chloride	CH_3HgCl	DI water pH approx 11	22	44	1.50×10^6	1, 3
methyl mercury chloride	CH_3HgCl	DI water pH approx 11	22	35	1.50×10^6	1, 3
methyl mercury chloride	CH_3HgCl	DI water pH approx 11	22	31	1.50×10^6	1, 3
methyl mercury chloride	CH_3HgCl	DI water pH approx 11	40	256	5.50×10^6	1, 3
methyl mercury chloride	CH_3HgCl	DI water pH approx 11	40	177	5.50×10^6	1, 3
methyl mercury chloride	CH_3HgCl	DI water pH approx 11	40	198	5.50×10^6	1, 3
methyl mercury chloride	CH_3HgCl	DI water pH approx 11	40	131	5.50×10^6	1, 3
methyl mercury chloride	CH_3HgCl	DI water pH approx 11	60	806	6.50×10^6	1, 3
methyl mercury chloride	CH_3HgCl	DI water pH approx 11	60	371	6.50×10^6	1, 3
methyl mercury chloride	CH_3HgCl	DI water pH approx 11	60	310	6.50×10^6	1, 3
methyl mercury chloride	CH_3HgCl	DI water pH approx 7	22	19	1.50×10^6	1, 3
methyl mercury chloride	CH_3HgCl	DI water pH approx 7	22	15	1.50×10^6	1, 3
methyl mercury chloride	CH_3HgCl	DI water pH approx 7	40	299	5.75×10^6	1, 3
methyl mercury chloride	CH_3HgCl	DI water pH approx 7	40	207	5.75×10^6	1, 3
methyl mercury chloride	CH_3HgCl	DI water pH approx 7	60	304	6.63×10^6	1, 3
methyl mercury chloride	CH_3HgCl	DI water pH approx 7	60	267	6.63×10^6	1, 3
methyl mercury chloride	CH_3HgCl	DI water pH approx 4	22	27	1.50×10^6	1, 3
methyl mercury chloride	CH_3HgCl	DI water pH approx 4	22	43	1.50×10^6	1, 3
methyl mercury chloride	CH_3HgCl	DI water pH approx 4	40	406	5.75×10^6	1, 3
methyl mercury chloride	CH_3HgCl	DI water pH approx 4	40	194	5.75×10^6	1, 3

RAW DATA FOR HENRY'S LAW, VAPOR PRESUURE AND SOLUBILITY STUDY

compound	chemical formula	solution conditions	temperature (°C)	gas phase concentration (ng/mL as Hg)	liquid phase concentration (ng/mL as Hg)	notes
methyl mercury chloride	CH_3HgCl	DI water pH approx 4	60	606	7.26×10^6	1, 3
methyl mercury chloride	CH_3HgCl	DI water pH approx 4	60	301	7.26×10^6	1, 3
methyl mercury sulfate	CH_3HgSO_4	DI water pH approx 7	22	28	1.35×10^7	1, 3
methyl mercury sulfate	CH_3HgSO_4	DI water pH approx 7	22	40	1.35×10^7	1, 3
methyl mercury sulfate	CH_3HgSO_4	DI water pH approx 7	40	142	1.62×10^7	1, 3
methyl mercury sulfate	CH_3HgSO_4	DI water pH approx 7	40	157	1.62×10^7	1, 3
methyl mercury sulfate	CH_3HgSO_4	DI water pH approx 7	60	397	3.04×10^7	1, 3
methyl mercury sulfate	CH_3HgSO_4	DI water pH approx 7	60	378	3.04×10^7	1, 3
methyl mercury glycolate	$CH_3Hg\ C_2H_3O_3$	DI water pH approx 7	22	47	8.04×10^7	1, 3
methyl mercury glycolate	$CH_3Hg\ C_2H_3O_3$	DI water pH approx 7	22	44	8.04×10^7	1, 3
methyl mercury glycolate	$CH_3Hg\ C_2H_3O_3$	DI water pH approx 7	40	1183	1.01×10^8	1, 3
methyl mercury glycolate	$CH_3Hg\ C_2H_3O_3$	DI water pH approx 7	40	1183	1.01×10^8	1, 3
methyl mercury glycolate	$CH_3Hg\ C_2H_3O_3$	DI water pH approx 7	60	2233	1.14×10^8	1, 3
methyl mercury glycolate	$CH_3Hg\ C_2H_3O_3$	DI water pH approx 7	60	3001	1.14×10^8	1, 3
methyl mercury hydroxide	CH_3HgOH	medium ionic strength (approx 0.51M OH^-)	22	16	1.00×10^8	1, 2
methyl mercury hydroxide	CH_3HgOH	medium ionic strength (approx 0.51M OH^-)	22	17	1.00×10^8	1, 2
methyl mercury hydroxide	CH_3HgOH	medium ionic strength (approx 0.51M OH^-)	40	480	1.00×10^8	1, 2
methyl mercury hydroxide	CH_3HgOH	medium ionic strength (approx 0.51M OH^-)	40	319	1.00×10^8	1, 2
methyl mercury hydroxide	CH_3HgOH	medium ionic strength (approx 0.51M OH^-)	60	1079	1.00×10^8	1, 2
methyl mercury hydroxide	CH_3HgOH	medium ionic strength (approx 0.51M OH^-)	60	1026	1.00×10^8	1, 2
methyl mercury hydroxide	CH_3HgOH	high ionic strength (approx 1.51M OH^-)	22	47	1.00×10^8	1, 2
methyl mercury hydroxide	CH_3HgOH	high ionic strength (approx 1.51M OH^-)	22	44	1.00×10^8	1, 2
methyl mercury hydroxide	CH_3HgOH	high ionic strength (approx 1.51M OH^-)	40	251	1.00×10^8	1, 2
methyl mercury hydroxide	CH_3HgOH	high ionic strength (approx 1.51M OH^-)	40	491	1.00×10^8	1, 2
methyl mercury hydroxide	CH_3HgOH	high ionic strength (approx 1.51M OH^-)	60	1135	1.00×10^8	1, 2
methyl mercury hydroxide	CH_3HgOH	high ionic strength (approx 1.51M OH^-)	60	2627	1.00×10^8	1, 2

notes:
1 -- initial concentration in vial was 0.5M (a 1:1 dilution of a 1M CH3HgOH solution in DI water) - total target concentration was 1.00E+08 ng/mL in solution
2 - no precipitation occurred; the measured liquid concentrations clustered tightly around the expected value and averaged 1.00E+08. This average was used in calcuati
3 -- precipitation occurred; the measured values for each temperature were tightly clustered and the average value for each temperatrue was used in the callculations

Distribution:

Records Administration (EDWS)

DOE Office of Scientific and Technical Information (OSTI)

tony.polk@srs.gov
nixon.peralta@srs.gov
Ombreyan.Broadwater@srs.gov
billy.hudson@srs.gov
jeffrey.crenshaw@srs.gov
james.folk@srs.gov

todd.shrader@em.doe.gov
Kurt.Gerdes@em.doe.gov
Michael.norato@em.doe.gov
linda.suttora@em.doe.gov
ming.zhu@em.doe.gov
grover.chamberlain@em.doe.gov
gary.peterson@em.doe.gov
nicholas.machara@em.doe.gov

connie.herman@srnl.doe.gov
brady.lee@srnl.doe.gov
frank.pennebaker@srnl.doe.gov
Boyd.Wiedenman@srnl.doe.gov
cj.bannochie@srnl.doe.gov
alex.cozzi@srnl.doe.gov
a.fellinger@srnl.doe.gov
Brenda.Garcia-Diaz@srnl.doe.gov
dennis.jackson@srnl.doe.gov
Joseph.Manna@srnl.doe.gov
daniel.mccabe@srnl.doe.gov
Gregg.Morgan@srnl.doe.gov
Amy.Ramsey@srnl.doe.gov
William.Ramsey@SRNL.DOE.gov
eric.skidmore@srnl.doe.gov
michael.stone@srnl.doe.gov
chris.martino@srnl.doe.gov
sharon.marra@srnl.doe.gov
natraj.iyer@srnl.doe.gov
william.bates@srnl.doe.gov
carol.eddy-dilek@srnl.doe.gov
brian02.looney@srnl.doe.gov
christine.langton@srnl.doe.gov
steve.wach@srnl.doe.gov
allan.young@srnl.doe.gov

Patricia.suggs@srs.gov
Brad.Swanson@parsons.com
Kevin.Brotherton@srs.gov
Richard.Edwards@srs.gov
terri.fellinger@srs.gov
Joseph.fields@srs.gov
jeffrey.gillam@srs.gov
barbara.hamm@srs.gov
robert.hoeppel@srs.gov
Thomas.Huff@srs.gov
bill.holtzscheiter@srs.gov
Vijay.Jain@srs.gov
Jeremiah.Ledbetter@srs.gov
jeff.ray@srs.gov
Azadeh.Samadi-Dezfouli@srs.gov
hasmukh.shah@srs.gov
aaron.staub@srs.gov
celia.aponte@srs.gov
timothy.baughman@srs.gov
earl.brass@srs.gov
Azikiwe.hooker@srs.gov
lauryn.jamison@srs.gov
Ryan.McNew@srs.gov
phillip.norris@srs.gov
Christine.Ridgeway@srs.gov
arthur.wiggins@srs.gov
Kevin.Brotherton@srs.gov
Grace.Chen@srs.gov
thomas.colleran@srs.gov
Spencer.Isom@srs.gov
Maria.rios-armstrong@srs.gov